NASA Contractor Report 168038

Tile

(UTRC Report R82-915640-8)

DEVELOPMENT OF A LINEAR AERODYNAMIC ANALYSIS FOR UNSTEADY TRANSONIC CASCADES

Joseph M. Verdon and Joseph R. Caspar

United Technologies Research Center
East Hartford, CT 06108

NASA

National Aeronautics and
Space Administration

Lewis Research Center
Cleveland, Ohio 44135

October 1982

1. Report No. CR 168038	2. Government Accession No.	3. Recipient's Catalog No.
4. Title and Subtitle DEVELOPMENT OF A LINEAR AERODYNAMIC ANALYSIS FOR UNSTEADY TRANSONIC CASCADES		5. Report Date October 1982
		6. Performing Organization Code
7. Author(s) Joseph M. Verdon and Joseph R. Caspar		8. Performing Organization Report No. R82-915640-8
		10. Work Unit No.
9. Performing Organization Name and Address United Technologies Research Center Silver Lane East Hartford, CT 06108		11. Contract or Grant No NAS3-21981
		13. Type of Report and Period Covered Contractor Report
12. Sponsoring Agency Name and Address National Aeronautics and Space Administration Washington, D.C. 20546		14. Sponsoring Agency Code 510-55-12

15. Supplementary Notes

Final Report. Project Manager, John J. Adamczyk, Fluid Mechanics and Acoustics Division, NASA Lewis Research Center, Cleveland, OH 44135.

16. Abstract An unsteady potential flow analysis, which accounts for the effects of blade geometry and mean pressure rise or fall across the blade row, is being developed to predict the aerodynamic response to turbomachinery blade vibrations. Linear, variable-coefficient, unsteady equations are approximated using difference expressions determined from an implicit least-squares development and applicable on arbitrary grids. The resulting system of algebraic equations permits an efficient, direct (i.e., noniterative) unsteady solution. Under the present effort, revised aerodynamic and numerical models have been formulated to determine a first-order approximation to a weak solution of the full-potential equation for transonic flow. The aerodynamic model applies at reduced frequencies of order unity and includes the effect of shock motions in a linear frequency-domain formulation. The numerical model has been extended to accommodate type-dependent and rotated differencing, and so that shocks can be fitted into the unsteady solution. In the present report this approximation was implemented on a rectilinear-type cascade mesh with calculations presented for cascades of sharp-edged airfoils aligned with the mean flow, and shocks have been captured. Sample results are provided to illustrate the effects of blade geometry, inlet Mach number and vibration frequency on unsteady response.

17. Key Words (Suggested by Author(s)) Unsteady flow; Transonic flow; Two-dimensional, finite deflection, cascade; Small amplitude vibration; Implicit, least-squares, approximation	18. Distribution Statement Unclassified – Unlimited		
19. Security Classif. (of this report) Unclassified	20. Security Classif. (of this page) Unclassified	21. No. of Pages 79	22. Price*

* For sale by the National Technical Information Service, Springfield, Virginia 22151

NASA-C-168 (Rev. 6-71)

Development of a Linear Aerodynamic Analysis for
Unsteady Transonic Cascades

TABLE OF CONTENTS

LIST OF SYMBOLS

Note: All quantities are dimensionless. Lengths have been scaled with respect to blade chord, time with respect to the ratio of blade chord to upstream free-stream speed, and pressure with respect to the upstream free-stream dynamic pressure.

Latin

$\boldsymbol{\alpha}$	matrix defining the least-squares fit, Eq. (62)
A_i, B_i, C_i, D_i, F_i	submatrices of block-quadridiagonal system of algebraic equations, Eq. (66)
$\hat{A}$	speed of sound, Eq. (2)
A	zeroth-order or steady speed of sound, Eq. (16)
$a e^{i\omega t}$	first-order or unsteady speed of sound, Eq. (22)
$\boldsymbol{\mathcal{B}}$	instantaneous position of blade surface; matrix defining the least-squares fit, Eq. (62)
B	mean position of blade surface, Fig. 1
$b_{j,\mp}$	far-field Fourier coefficient, Eq. (35)
$\boldsymbol{C}$	interpolating matrix, Eq. (63)
C^{ν}	variable coefficient which depends on the steady flow, Eq. (46)
$\hat{\vec{C}}_F, \hat{C}_M$	aerodynamic force, moment coefficient, Eqs. (40) and (41)
$\vec{C}_F, C_M$	zeroth-order or steady force, moment coefficient, Eq. (42)
$\vec{c}_F, c_M$	first-order or unsteady force, moment coefficient, Eq. (43)
c_L	unsteady lift coefficient
$\boldsymbol{\mathcal{D}}$	extended blade passage solution domain, Fig. 2
$\boldsymbol{\mathcal{D}}_{\nu}$	linear differential operator, Eq. (45)

$\vec{n}$ unit normal vector directed outward from blade surfaces, upward at wakes, and downstream at shocks

$\mathcal{O}$ order symbol

$\hat{P}$ pressure, Eq. (2)

P zeroth-order or steady pressure, Eq. (16)

$\bar{P}$ steady perturbation pressure, Eq. (A9)

$pe^{i\omega t}$ first-order or unsteady pressure, Eq. (22)

Q_m mesh point, m = 0 refers to calculation point, m = 1, ..., M refers to neighboring mesh points

q^0 multiplicative constant, Eq. (56)

q_j far-field constant, Eq. (34)

$\mathcal{R}$ blade, Eq. (4), wake, or shock, Eq. (8), displacement vector

R radius of curvature of DCA blade surface, Eq. (68)

$\vec{R}_p$ position vector extending from the mean position of the reference blade axis of rotation to points on the mean position of the reference blade surface, Eq. (6)

Re { }   real part of { }

$\vec{r}$ blade-displacement amplitude vector, Eq. (6)

r amplitude of shock displacement normal to the shock mean position, Eq. (29)

$\hat{S}$ entropy

S,N   local canonical Cartesian coordinates with S-axis directed along steady streamline, Eq. (49)

$\mathcal{S}h$ instantaneous position of shock surface

Sh   mean position of shock surface, Fig. 1

t   time

$\vec{V}$	zeroth-order or steady velocity
$\mathcal{W}$	instantaneous position of wake surface
W	mean position of wake surface, Fig. 1; diagonal weighting function matrix with components, W_m, $m = 1, \ldots, M_1$, Eqs. (59) and (62)
$\hat{\vec{X}}$	position vector in blade-fixed coordinate frame, Eq. (10)
$\vec{X}$	position vector in space-fixed coordinate frame, Eq. (10)
X_p, Y_p	coordinates of mean position of reference blade pitching (torsional) axis
x, y	space-fixed Cartesian coordinates with x-axis directed along mean position of reference blade chord line, Fig. 1

Greek

$\vec{\alpha}$	rotational displacement vector, Eq. (6)
$\underset{\sim}{\beta}$	column vector of difference coefficients β_m, $m = 1, \ldots, M$, Eq. (65)
$\underset{\sim}{\gamma}$	column vector of interpolating coefficients γ_n, $n = 1, \ldots, N$, Eq. (55)
γ	specific heat ratio
Δp	unsteady pressure difference coefficient, Eq. (69)
$\bar{\delta}, \delta$	thin-airfoil characteristic lengths, Eq. (A1)
$\delta\xi, \delta\eta$	axial, tangential (i.e., parallel to the cascade inlet plane) distance between mesh points
$\delta\phi_m$	difference between values of ϕ at mth neighbor point and at calculation point, Eq. (60)
$\underset{\sim}{\delta\phi}$	column vector with components $\delta\phi_m$, $m = 1, \ldots, M$, Eq. (61)
$\varepsilon, \bar{\varepsilon}$	small parameters, Eqs. (10) and (A2)
η_+	η-coordinate of the point of intersection of the reference stagnation streamline and the axial line $\xi = \xi_+$, Fig. 2 and Eq. (36)

Θ	cascade stagger angle, Fig. 1
λ	coordinate scaling parameter, Eq. (A4)
ξ, η	space-fixed Cartesian coordinates with ξ-axis directed axially and downstream, Fig. 1
$\xi_{\mp}$	ξ-coordinates of far upstream and downstream boundaries, Fig. 2
$\hat{\rho}$	fluid density, Eq. (2)
$\bar{\rho}$	zeroth-order or steady density, Eq. (16)
$\rho e^{i\omega t}$	first-order or unsteady density, Eq. (22)
$\vec{\tau}$	unit vector tangent to blade, wake, or shock surface and directed such that $\vec{n} \times \vec{\tau} = \vec{e}_z$
τ, η	space-fixed Cartesian coordinates with τ-axis directed along the mean position of the reference wake, Fig. 1
$\hat{\phi}$	velocity potential, Eq. (1)
Φ	zeroth-order or steady velocity potential, Eq. (15)
$\bar{\phi}$	steady perturbation potential, Eq. (A2)
$\phi e^{i\omega t}$	first-order or unsteady velocity potential, Eq. (24)
$\phi_c e^{i\omega t}$	continuous component of far-field unsteady potential, Eq. (34)
$\phi_d e^{i\omega t}$	disconponent component of far-field unsteady potential, Eq. (36)
$\chi_{j,\pm}$	far-field constant, Eq. (34)
Ω	steady far-field flow angle, Fig. 1
ω	frequency (circular) of blade motion, Eq. (5)

Superscripts

n	component of column vector
T	transpose
——	complex conjugate

*	conjugate transposition

Subscripts

$\mathfrak{B}$	instantaneous position of blade surface, Eq. (37)
B	mean position of blade surface, Eq. (37)
I	number of axial mesh lines
i,j	axial, tangential mesh line
M	number of neighbor points
m	blade number; neighboring mesh point
$\mathscr{S}$	instantaneous position of blade, wake or shock surface, Eq. (11)
S	mean position of blade, wake, or shock surface, Eq. (11)
t	local time derivative
x, y, ξ, η, τ, n	vector component or partial derivative in indicated direction
0	calculation point
+, -	upper, lower surface of blade or wake; downstream, upstream of blade row
$\mp\infty$	far upstream, downstream of blade row
$\sim$	column vector

LIST OF FIGURES

Development of a Linear Aerodynamic Analysis for Unsteady Transonic Cascades

SUMMARY

A linear unsteady potential flow analysis, which accounts for the effects of blade geometry and mean pressure rise or fall across the blade row, is being developed to predict the aerodynamic response to blade vibrations in the fan, compressor, or turbine stages of jet engines. Based on the assumption of small-amplitude blade motions, the unsteady flow is governed by linear equations with variable coefficients which depend on the underlying steady flow. These equations are approximated using difference expressions determined from an implicit least-squares development and applicable on arbitrary grids. The resulting system of linear algebraic equations permits an efficient, direct (i.e., noniterative) solution to the linear unsteady boundary value problem. In previous work unsteady solutions were determined for subsonic cascades of blunt-nosed airfoils by matching an "outer" solution, determined on a rectilinear-type cascade mesh which spans an extended blade passage region, to an "inner" solution, determined on a polar-type local mesh which surrounds a blade leading edge. In the present effort the unsteady aerodynamic analysis is being extended for transonic applications.

Revised aerodynamic and numerical models have been formulated to determine a first-order approximation to a weak solution (i.e., a solution admitting discontinuities) of the time-dependent, full-potential equation for small-amplitude, harmonic, blade motions. The aerodynamic model is intended for application at reduced frequencies of order unity or lower - an important feature for turbomachinery applications - and includes the effect of shock motions in a linear frequency-domain calculation. The implicit, least-squares, numerical approximation has been extended to accommodate type-dependent and rotated differencing strategies in supersonic regions and at the interfaces between subsonic and supersonic regions, and to fit shocks into the unsteady flow field. In the present report, this approximation has been implemented on the cascade mesh and calculations are presented for cascades of sharp-edged airfoils with blade mean positions aligned with the mean or steady flow. Shocks have been "captured" in the finite difference approximation as smooth regions in which the flow variables are rapidly but continuously varying. Results are presented here for unstaggered and staggered cascades to demonstrate the present capability and to partially illustrate the effects of blade geometry, Mach number, and vibration frequency on unsteady response.

INTRODUCTION

In transonic flow relatively small-amplitude unsteady motions can produce larg
variations in the magnitude and phase of the aerodynamic forces and moments. These
characteristics enhance the likelihood of an aeroelastic instability and thus are a
major concern in the aerodynamic design of configurations that operate in the
transonic regime. Of particular concern are aeroelastic behavior and flutter
boundaries. Although much progress has been made in the development of unsteady
transonic computational methods for the aeroelastic analysis of two-dimensional,
isolated airfoils (c.f., Ref. 1), relatively little attention has been focused on
the development of such methods for turbomachinery blade rows (c.f., Ref. 2). Thus
the objective of the present effort is to develop a reliable and efficient procedur
for predicting the forces and moments acting on the oscillating blades of a two-
dimensional cascade operating at transonic Mach numbers. Although the interest her
is focused on cascades, the basic aerodynamic model described in this report shoul
also provide an efficient method for calculating the unsteady forces associated wit
the motions of a variety of aerodynamic configurations including those of thick,
blunt-nosed, transonic airfoils.

Background

Unsteady Transonic Flow Models

Three different potential flow models have and are being extensively developed
to treat unsteady transonic flow past two-dimensional, isolated airfoils. These
include: (1) a linear, low frequency, very small, unsteady disturbance approxima-
tion (Refs. 3-6); (2) a nonlinear, low frequency, small-disturbance approximation
(Refs. 7-8); and (3) analyses based on the time-dependent, full-potential equation
(Refs. 9-11). In proceeding from the first to the third of these models more of th
physics of unsteady transonic phenomena is captured, but computational complexity
and the cost of obtaining unsteady predictions is increased.

In the first approach, often referred to as the "time-linearized" unsteady
transonic approximation, the amplitudes and frequency of the unsteady perturbations
are assumed to be small compared to steady velocity perturbations caused by airfoil
shape and incidence. Steady perturbations are, in turn, assumed to be small com-
pared to the uniform stream speed. Both frequency- (Refs. 3-5) and time-domain
(Ref. 6), time-linearized, unsteady, transonic solutions can be determined with
relatively little expenditure of computer time. A serious limitation of the fre-
quency-domain calculations has been the neglect of shock wave motions. The amplitu
of such motions increases with the amplitude of the airfoil motion and decreases wi
frequency. Shock motions can contribute substantially to the time varying load,
especially at low frequency, and must be considered in computing unsteady solutions
correctly to lowest order. Fung, Yu and Seebass (Ref. 6) have recently provided a

method to account for shock motions within the time-linearized formulation and to calculate both indicial and harmonic responses due to small unsteady changes in boundary conditions using an implicit, time-marching, finite-difference approximation.

The restrictions imposed by the time-linearized, unsteady, transonic approximation; i.e., that unsteady perturbations are small compared to steady perturbations, and the neglect of shock motions in the earlier time-linearized solutions, have led to the development of an alternative small-disturbance approximation (Refs. 7, 8). In this second approach, steady and low-frequency unsteady disturbances to the free stream are assumed to be of the same order and small relative to the free-stream speed, resulting in a time-dependent, nonlinear, differential equation governing the disturbance potential. An implicit time-marching, finite difference approximation and computer code (LTRAN2) have been developed for determining indicial responses, and predictions have been found to be in qualitative agreement with Tijdemann's (Ref. 12) experimental observations on shock motions. Although the nonlinear, transonic, small-disturbance approximation is formally valid only at low frequency, high frequency versions of the LTRAN2 code have recently been developed to analyze unsteady transonic flows past isolated airfoils (Refs. 13 and 14) and two-dimensional unstaggered cascades (Ref. 15).

Simple treatment of arbitrary airfoils and airfoil motions is the principal advantage of the transonic small-disturbance formulations. Airfoil and wake boundary conditions are imposed on a flat, mean-surface approximation to the air-foil and wake; however, the assumptions that permit this simplification place severe restrictions on airfoil shape and on the amplitude and frequency of the airfoil motion. Restrictions on the amplitude of the motion may not detract from the usefulness of the small disturbance concept for most aeroelastic applications, but those placed on frequency and airfoil geometry do pose serious limitations, particularly for the thick, blunt-nosed profiles which are a common feature of transonic designs. To overcome these geometric and kinematic limitations, several researchers are developing time-dependent, full-potential analyses for unsteady, transonic, airfoil applications.

Isogai (Ref. 9) was the first to apply the time-dependent, full-potential equation to investigate the feasibility of treating thick, blunt-nosed airfoils. His approach is essentially a hybrid one. Although the time-dependent, full-potential equation is taken as the governing differential equation, airfoil and wake boundary conditions are applied on the time-mean position of the airfoil surface and on the x-axis, respectively. Thus, small-amplitude motions are implicitly assumed, but boundary conditions are satisfied on the actual mean surface of the airfoil rather than on a flat, mean-surface approximation. Isogai solved the full potential equation in nonconservative form using a time-marching, semi-implicit, finite-difference procedure and a quasi-conservative scheme to capture shock motions. Computed results for a NACA 64A006 airfoil compare well with the corresponding shadowgraph observations made by Tijdeman (Ref. 12).

3

With a view towards improving the computational efficiency and shock capturing capability of Isogai's method and removing the small unsteady disturbance restriction Chipman and Jameson (Ref. 10) and Goorjian (Ref. 11) are developing complete full potential formulations. In their work, the full, nonlinear, time-dependent, governing equations are expressed in time-dependent coordinates so that flow tangency boundary conditions can be imposed directly on moving airfoil surfaces. Chipman and Jameson solve a system of first-order equations written in full conservation form in terms of primitive variables. These equations are transformed to a time-varying, sheared, rectilinear, coordinate system. Both explicit and implicit, time-marching, finite-difference schemes have been coded. Goorjian has developed an algorithm for solving the conservative form of the full-potential equation expressed in general, time-varying, curvilinear coordinates by an alternating direction, fully-implicit method. The feasibility and accuracy of these approaches have been demonstrated for several simple geometries including ones for which exceedingly large shock excursions occur.

The full potential formulations of Refs. 10 and 11 represent very sophisticated numerical analyses for revealing the physical features of unsteady transonic flows. With further development these models should provide "benchmark" unsteady transonic flow calculations, particularly for finite-amplitude unsteady motions. However, the computing time requirements for these analyses will prohibit their routine use in detailed aeroelastic investigations. The needs of the aeroelastician could perhaps be better met by a linear, unsteady, small-disturbance, potential-flow formulation which includes the effects of real airfoil geometry and moderate to high vibration frequencies on unsteady response but still permits efficient numerical solutions. The purpose of the present investigation is to provide such an unsteady analysis for turbomachinery aeroelastic applications.

Unsteady Cascade Analyses

The unsteady aerodynamic analyses currently used for turbomachinery aeroelastic studies (see Ref. 16 for an informative review) are based on classical linear aerodynamic theory; i.e., the unsteady flow is essentially regarded as a small fluctuation about uniform steady flow. Such analyses only apply in entirely subsonic or entirely supersonic flow and neglect the effects of blade shape, mean incidence, and mean pressure rise or fall across the blade row. As such, classical linear unsteady solutions fail to meet the requirements of turbomachinery designers over a wide range of practical operating conditions.

To partially overcome the limitations of classical linear theory, subsonic unsteady aerodynamic models have been formulated (Refs. 17-20) which include the effects of blade geometry and steady flow turning on unsteady response. Here the unsteady flow is considered as a small-amplitude harmonic fluctuation about fully nonuniform steady flow. An asymptotic expansion of the time-dependent velocity potential then provides equations which govern the steady and small-disturbance unsteady flows in a single, extended, blade-passage region of the cascade. The steady flow is determined as a solution of the full-potential equation, and the unsteady flow is governed by linear

equations with variable coefficients which depend on the underlying steady flow. With this formulation a numerical resolution of a time-independent, unsteady, boundary-value problem is required only over a single blade-passage region or finite extent.

Several accurate and reliable numerical algorithms for solving the nonlinear, steady problem for subsonic or transonic cascade flow are currently available (c.f., Ref. 21). A finite-difference approximation based on an implicit least-squares development and applicable on arbitrary grids has been reported by the present authors for resolving the subsonic, linear, unsteady problem (Ref. 22). This approximation has been implemented on a rectilinear-type, body-fitted, and periodic grid, called the "cascade" grid, to predict the unsteady flow in an extended blade-passage region and on a dense, polar-type local grid to determine the unsteady flow in the vicinity of a blunt leading edge. In previous studies subsonic unsteady solutions have been determined for cascades of sharp-edged airfoils with mean positions aligned with the steady flow (Refs. 17, 22) and for cascades of NACA 0012 airfoils (Refs. 23, 24), both to demonstrate the unsteady solution capability and to illustrate the effects of blade geometry (including leading-edge curvature), mean incidence, compressibility, and vibration frequency on unsteady response. Our results to date have indicated that blade thickness produces a strong coupling between the steady and unsteady flows, particularly at high subsonic Mach number and/or low vibration frequency, but that steady turning due to mean incidence or camber produced only weak steady/unsteady interactions. Recently, unsteady pressure-difference predictions for a cascade of NACA 65 series airfoils operating at low Mach number and frequency have been shown to be in excellent agreement with cascade wind tunnel measurements obtained by Carta (Ref. 25).

Scope of the Present Investigation

The objective of the present effort is to extend the foregoing unsteady aero-dynamic analysis for cascades operating in the transonic Mach number regime. The aerodynamic model of Refs. 17 and 24 has been extended for transonic applications by introducing shock jump conditions into the full-potential, nonlinear, steady, and the linear, unsteady, boundary-value problems. The first-order shock-jump conditions provide relations for determining the discontinuous change in the unsteady flow quantities across a shock as well as the amplitude of the shock motion. These conditions are derived from the integral form of the mass conservation law, and either the integral form of the conservation law for the component of fluid momentum tangent to the shock or the requirement that no vorticity can be produced at the shock. Further, the implicit-interpolation, numerical approximation described in Ref. 22 for the resolution of unsteady subsonic cascade flows has been modified for transonic applications by incorporating the rotated and type-dependent differencing concepts introduced by Jameson (Ref. 26) and Murman and Cole (Refs. 27 and 28), respectively. Thus, at each point of the finite difference mesh the unsteady equation

is expressed in canonical form. In this form it becomes readily apparent that the local character of the unsteady equation depends only on the local steady Mach number. Difference approximations to the second derivative of the unsteady potenti; the streamwise direction at a given point depend on whether the unsteady differenti; equation is locally elliptic (subsonic flow), parabolic (sonic flow) or hyperbolic (supersonic flow). At shocks first-order, shock-jump conditions are applied with normal (to the shock) derivative terms approximated by one-sided differences on either side of the shock.

With the present unsteady transonic formulation we seek a first-order approximation to a weak solution (i.e., a solution admitting discontinuities) of the time-dependent, full-potential equation for small-amplitude harmonic blade motions. The nonconservative form of the unsteady differential equation is solved in regions where the flow variables are continuous, and jump conditions are applied at surfaces across which flow variables are discontinuous (shocks and blade wakes). Hence, discontinuities are removed from the finite difference domain and "fitted" into the overall unsteady solution. This unsteady formulation applies at reduced frequencies of order unity or lower, and includes the effect of shock motions in a linear, frequency-domain calculation. Finally, numerical results are obtained by direct inversion of the resulting set of difference equations, and hence, iterative solution procedures are not required.

Thus the present analysis differs in several important respects from the time-linearized analyses which have been developed for the prediction of unsteady transonic flows past isolated airfoils (Refs. 3-6). The latter assume that steady and unsteady disturbances due to airfoil shape and motion are small and very small, respectively, relative to the uniform stream speed. As a result, the unsteady equation formally applies only in the limit of low-frequency airfoil motions (c.f. the Appendix to this report). In the frequency-domain calculations of Refs. 3-5, the unsteady equation is solved in nonconservative form, but shocks are "captured" as smooth rapidly varying regions in the finite difference approximation and shock motions are ignored. In the time-domain calculation of Ref. 6, the unsteady transonic equation is solved in conservative form. Shocks are "fitted" as discontinuities, and shock motions are accounted for; however, an iterative, time-marching, procedure is required to achieve unsteady solutions.

In this report the unsteady transonic aerodynamic model and numerical approximation are described, and numerical results are presented and evaluated for cascades of vibrating, sharp-edged, double-circular-arc (DCA) airfoils, with mean positions aligned with the steady flow. This simple blade geometry has been selected so that at this, the first stage of our unsteady transonic investigation, we could concentrate on the transonic aspects of the problem (i.e., local supersonic regions and shock discontinuities) without having to deal with the complications introduced by mean incidence or steady flow stagnation at blade leading and trailing edges. At present the unsteady transonic numerical approximation has

been implemented only on the cascade mesh. Our experience indicates that shock-jump conditions cannot be accurately modeled on this mesh, and hence, although the intent is to eventually fit shocks into the unsteady solution, the transonic results presented here have been determined by shock capturing. In addition, cascade mesh solutions deteriorate in the vicinity of a shock with increasing blade stagger due to a greater number of axial mesh lines crossing the shock. Work is currently underway to implement the numerical approximation on a detailed local mesh containing the shock to permit accurate shock fitting and an improved resolution of unsteady flows past staggered cascades.

THE POTENTIAL FLOW AERODYNAMIC MODEL

Basic equations which describe the flow past a finite-deflection, two dimensional, oscillating cascade of airfoils are presented below. In the present effort we seek solutions to the unsteady boundary value problem for transonic flows; i.e., flows with subsonic inlet and exit conditions, but with embedded supersonic regions adjacent to blade surfaces. In the following discussion all quantities are dimensionless. Lengths have been scaled with respect to blade chord, time with respect to the ratio of blade chord to upstream free-stream speed, and pressure with respect to the upstream free-stream dynamic pressure.

We consider adiabatic flow, with negligible body forces, of an inviscid, non-heat conducting, perfect gas past a two-dimensional oscillating cascade (Fig. 1). The mean or steady-state positions of the blade chord lines coincide with the line segments $mG_x \leq x \leq 1 + mG_x$, $y = mG_y$, $m = 0 \pm 1, \pm 2, \ldots$, where m is a blade number index, and G_x and G_y are the x and y components of the cascade gap vector $\vec{G}$, which is directed along the locus of blade leading edges with magnitude equal to the blade spacing (Fig. 1). It is assumed that in the absence of blade motions uniform subsonic inlet and exit conditions exist far upstream and downstream of the blade row. The blades are undergoing identical harmonic motions at frequency, ω, and with constant phase angle, σ, between the motion of adjacent blades. Blade shape and orientation relative to the inlet free stream and the amplitude, frequency, and mode of the blade motion are assumed to be such that the flow remains attached to the blade surfaces. Thus, thin vortex sheets (unsteady wakes) emanate from the blade trailing edges and extend downstream. In addition, for sufficiently high subsonic inlet conditions, local supersonic regions which terminate at moving shocks will occur adjacent to blade surfaces.

Time-Dependent Full-Potential Formulation

Equations governing the fluid motion can be derived from the integral conservation laws for mass, momentum and energy, and the thermodynamic equation of state. These integral laws provide corresponding differential equations in regions of the fluid where the flow variables are continuously differentiable and "jump" conditions at surfaces across which (in the inviscid approximation) the flow variables are discontinuous; i.e., shocks and blade wakes. In continuous regions of the flow the energy equation can be replaced by the requirement that the entropy, $\hat{S}$, following a fluid particle must remain constant; i.e., $D\hat{S}/Dt = 0$ (Ref. 29). In general, the discontinuous changes in the flow quantities across shocks are proportional to the shock strength, but the increase in entropy across the shock is proportional only to the third power of shock strength (Ref. 30). Thus for shocks of weak to moderate strength it is a reasonable approximation to neglect changes in entropy across the shock. With this approximation, the uniform undisturbed flow far upstream of the cascade will produce an isentropic ($\hat{S} = S_{-\infty}$) and hence by the Helmholtz theorem, an irrotational, time-dependent flow field.

Governing Differential Equation

The mass conservation law provides the following conservative form of the differential equation

$$\frac{\partial \hat{\rho}}{\partial t} + \nabla \cdot (\hat{\rho} \nabla \hat{\Phi}) = 0 \tag{1}$$

where t is time, governing the fluid density, $\hat{\rho}$, and velocity potential, $\hat{\Phi}$. In addition, after substituting the isentropic relations into the differential form of the momentum conservation law and integrating the resulting expression, the following relations (Burnoulli's equation) between the flow variables are obtained

$$\hat{\rho}^{(\gamma-1)} = (\gamma M_{-\infty}^2 \hat{P}/2)^{(\gamma-1)/\gamma} = (M_{-\infty} \hat{A})^2$$
$$= 1 - (\gamma-1) M_{-\infty}^2 \left\{ \hat{\Phi}_t + \left[(\nabla \hat{\Phi})^2 - 1 \right]/2 \right\} \tag{2}$$

Here γ is the specific heat ratio of the fluid, M is the Mach number of the undisturbed or steady flow, $\hat{P}$ is the fluid pressure, $\hat{A}$ is the speed of sound propagation, and the subscript $-\infty$ refers to the upstream free-stream condition. If the dependence of the density on the velocity potential is explicitly included, using Eq. (2), the potential equation, Eq. (1), can be written in the form

$$\hat{A}^2 \nabla^2 \hat{\Phi} = \hat{\Phi}_{tt} + 2\nabla\hat{\Phi} \cdot \nabla\hat{\Phi}_t + \nabla\hat{\Phi} \cdot \nabla(\nabla\hat{\Phi})^2/2 \tag{3}$$

Equation (3) is the nonconservative form of the differential equation which governs the time-dependent velocity potential in continuous regions of the flow. Since, by assumption, unsteady disturbances are produced solely by the blade motion, the admissable solutions of either Eq. (1) or Eq. (3) for the present application are those in which far-field acoustic energy radiates away from the blade row. Blade motions are then classified as subresonant if acoustic energy attenuates in the far field, or as superresonant if acoustic waves persist far upstream and/or downstream of the blade row.

Surface Conditions

The foregoing equations are supplemented by boundary conditions on moving blade surfaces, $\mathcal{B}_m$, and jump conditions at moving blade wakes, $\mathcal{W}_m$, and at moving shocks $\mathcal{S}h_{m,\pm}$, where the subscript + or - refers to a shock impinging on the upper or lower surface, respectively, of the mth blade. The vectors $\vec{\mathcal{R}}$, $\vec{n}$, and $\vec{\tau}$ are introduced below in conjunction with the surface conditions. The relative displacement vector, $\vec{\mathcal{R}}$, measures the displacement of a point on the instantaneous position of a surface (blade, wake, or shock) relative to its mean or steady-state position. The unit vectors $\vec{n}$ and $\vec{\tau}$ are normal and tangent, respectively, to a surface and directed such tha $\vec{n} \times \vec{\tau} = \vec{e}_z$ points out from the page. The unit normal vector is directed outward from blade surfaces, upward at wakes, and downstream at shocks.

For attached flows, the normal component of the fluid velocity must equal the normal component of the surface velocity at blade surfaces (flow tangency); i.e.,

$$(\nabla\hat{\phi}\cdot\vec{n}) = \frac{\partial\vec{\mathcal{R}}}{\partial t}\cdot\vec{n}, \qquad \text{on } \mathcal{B}_m \qquad (4)$$

Due to the assumed form of the blade motions

$$\vec{\mathcal{R}}(\vec{X}+m\vec{G},t) = \vec{r}(\vec{X})e^{i(\omega t + m\sigma)}, \qquad \vec{X} \text{ on } B \qquad (5)$$

where the vector $\vec{r}$ is prescribed and defines the amplitude and direction of blade displacements, $\vec{X}$ is a position vector in the space-fixed x,y-coordinate frame, and B denotes the mean position of the zeroth or reference blade. For rigid blade motions

$$\vec{r}(\vec{X}) = \vec{h} + \vec{\alpha} \times \vec{R}_p - (1-\cos\alpha)\vec{R}_p \qquad (6)$$

where $\vec{h}$ defines the amplitude and direction of blade translations, $\vec{\alpha}$ defines the amplitude and direction (positive counterclockwise) of blade rotations, and $\vec{R}_p$ is a position vector extending from the mean position of the reference-blade axis of rotation to points on the mean position of the reference blade surface. The components h_x, h_y and α of the vectors $\vec{h}$ and $\vec{\alpha}$ are, in general, complex to permit phase differences between the translations in the x and y-directions and the rotation These rigid two-dimensional motions model bending and torsional vibrations of actual rotor blades.

The blade wakes are material surfaces; i.e., a fluid particle on the wake always remains there. Hence, Eq. (4) also applies at wake surfaces. However, since the wake displacement vector is unknown apriori, "jump" conditions are usually imposed at wake surfaces. It follows from the foregoing kinematic condition and the integral conservation laws that the component of fluid velocity normal to the wake and the thermodynamic properties of the fluid must be continuous across thin vortex wakes. Thus, the conditions

$$[\![\nabla\hat{\phi}]\!]\cdot\vec{n} = [\![\hat{p}]\!] = 0, \qquad \text{on } \mathcal{W}_m \qquad (7)$$

apply at wake surfaces, where $[\![\ ]\!]$ denotes the difference (upper minus lower) in a quantity across a wake. Since the instantaneous wake locations, $\mathcal{W}_m$, are unknown, the usual practice is to apply these continuity conditions on prescribed surfaces which lie close to the actual wake positions.

At shocks the integral form of the mass conservation law provides the following condition

$$[\![\hat{p}(\nabla\hat{\phi} - \frac{\partial\vec{\mathcal{R}}}{\partial t})]\!]\cdot\vec{n} = 0, \qquad \text{on } \mathcal{S}h_{m,\pm} \qquad (8)$$

where $[\![\quad]\!]$ denotes the jump or difference (downstream minus upstream) in a quantity across a shock. A second shock-jump condition follows from the conservation of momentum tangent to the shock and requires that the component of fluid velocity tangent to the shock, or after integrating along the shock that the velocity potential, must be continuous across the shock; i.e.,

$$\vec{\tau} \cdot [\![\nabla \hat{\phi}]\!] = [\![\hat{\phi}]\!] = 0 \quad , \qquad \text{on } \mathscr{S}h_{m,\pm} \tag{9}$$

Equation (9) also represents the requirement that no vorticity be produced at the shock. In isentropic flow, if mass conservation is required, then neither the normal component of fluid momentum nor energy can be conserved across the shock.

This completes the formulation of the boundary value problem for the velocity potential, $\hat{\phi}$. The problem posed is a formidable one consisting of a nonlinear, time-dependent, partial differential equation along with conditions imposed on moving blade, shock and wake surfaces, in which the instantaneous locations of shock and wake surfaces must, in principle, be determined as part of the solution. Even if accurate solution procedures could be developed for this problem, they would be of limited value to the designer because computing time requirements would make it prohibitively expensive to obtain the unsteady response predictions required for detailed flutter calculations. Thus the approximation described below has been developed to provide a useful analytical model for turbomachinery aeroelastic investigations.

THE SMALL UNSTEADY DISTURBANCE APPROXIMATION

If the amplitude of the blade motion is small; i.e., $|\vec{r}| \sim \mathcal{O}(\varepsilon)$ where ε is a small parameter, a perturbation analysis can be applied to replace the foregoing nonlinear, time-dependent, boundary-value problem by two time-independent problems for the zeroth-order or steady flow field and the first-order, harmonic (in time), unsteady flow field. In addition, within the first-order approximation, unsteady boundary conditions can be applied at the mean positions of blade, B_m, wake, W_m, and shock, $Sh_{m,\pm}$, surfaces and blade pressure distributions and aerodynamic response coefficients can be evaluated in terms of information supplied at blade mean positions. The mean positions of the blade wakes and the shocks are determined by the steady solution, which is assumed to be known in the present study.

Flow quantities are first expanded in asymptotic series in ε; e.g.,

$$\hat{\Phi}(\hat{\vec{X}},t) = \sum_{j=0}^{j} \epsilon^j \phi_j(\hat{\vec{X}},t) = \Phi(\vec{X}) + \phi(\vec{X})e^{i\omega t} + \mathcal{O}(\epsilon)^2 \tag{10}$$

where $\hat{\vec{X}}$ is a position vector measured relative to body-fixed Cartesian coordinates which coincide with the space-fixed x,y-coordinates when the reference blade (m = 0) is in its mean position. In addition, Taylor series expansions; e.g.,

$$\nabla\hat{\Phi}\Big|_{\mathcal{B}} = \nabla\hat{\Phi}\Big|_S + (\vec{\mathcal{R}}\cdot\nabla)\nabla\hat{\Phi}\Big|_S + \mathcal{O}(\epsilon^2) \tag{11}$$

where $\mathcal{B}$ denotes a moving blade, wake, or shock surface, S denotes the mean position of this surface and $\vec{\mathcal{R}}$ defines the displacement between corresponding points on the moving and mean surfaces, are applied to refer boundary conditions to the mean surface positions. Unit tangent and normal vectors at a point on a moving surface are related to the unit tangent and normal vectors at the corresponding point on the mean surface by the relations

$$\vec{\tau}_{\mathcal{B}} = \vec{\tau}_S \left[1 - \vec{\tau}_S \cdot \nabla\mathcal{R}\cdot\vec{\tau}_S \right] + (\vec{\tau}_S\cdot\nabla)\vec{\mathcal{R}} + \mathcal{O}(\epsilon^2) \tag{12}$$

$$\vec{n}_{\mathcal{B}} = \vec{\tau}_S \times \vec{e}_z = \vec{n}_S \left[1 - \vec{\tau}_S\cdot\nabla\mathcal{R}\cdot\vec{\tau}_S \right] + (\vec{\tau}_S\cdot\nabla)\vec{\mathcal{R}} \times \vec{e}_z + \mathcal{O}(\epsilon^2)$$

In particular, for the rigid blade motions defined by Eq. (6)

$$\vec{\tau}_{\mathcal{B}} = \vec{\tau}_S - \alpha\vec{n}_S\, e^{i\omega t} + \mathcal{O}(\epsilon^2) \tag{13}$$

$$\vec{n}_{\mathcal{B}} = \vec{n}_S + \alpha\vec{\tau}_S\, e^{i\omega t} + \mathcal{O}(\epsilon^2)$$

After substituting the foregoing series and surface vector relations into the full governing equations, equating terms with like powers in ε, and neglecting terms of second and higher order in ε, nonlinear and linear, variable-coefficient, boundary-value problems are obtained, respectively, for the zeroth- and first-order flows.

As $\varepsilon \to 0$ the blade and wake surfaces collapse to their mean positions. Hence, the zeroth-order term in the power series expansion, Eq. (10), is the velocity potential, $\Phi(\vec{X})$, due to steady flow past a stationary cascade. The cascade geometry, the prescribed form of the blade motion, and the linearity of the first-order equations require that the first-order or unsteady potential be harmonic in time (i.e., $\varepsilon\Phi_1(\vec{X}, t) = \phi(\vec{X}) e^{i\omega t}$) and that both the steady and first-order unsteady flows exhibit blade-to-blade periodicity; i.e.,

$$\Phi(\vec{X}) = \Phi(\vec{X} + m\vec{G}) - m\vec{V}_{-\infty} \cdot \vec{G} \tag{14}$$

$$\phi(\vec{X}) = \phi(\vec{X} + m\vec{G})e^{-im\sigma}$$

The periodicity conditions permit numerical solutions for the steady and unsteady flows to be determined in a single, extended, blade-passage region of the cascade (e.g., the region $\mathscr{D}$ in Fig. 2). In addition, unsteady quantities at the mth blade, wake, or shock surface can be evaluated in terms of information provided at the reference (m = 0) blade, wake, or shock surface, respectively. For convenience the subscript m will be omitted below when referring to a reference surface.

The Steady Boundary Value Problem

Equations governing the steady flow follow from Eqs. (1) through (4), (8), and (9), after replacing the time-dependent flow quantities, $\hat{\Phi}$, $\hat{P}$, $\hat{\rho}$, and $\hat{A}$, by their zeroth-order or steady flow counterparts, Φ, P, $\bar{\rho}$, and A, and omitting time-derivative terms. Thus the differential equation

$$\nabla \cdot (\bar{\rho}\, \nabla\Phi) = A^2\nabla^2\Phi - \nabla\Phi \cdot \nabla(\nabla\Phi)^2/2 = 0 \tag{15}$$

where

$$\bar{\rho}^{(\gamma-1)} = (\gamma M_{-\infty}^2 P/2)^{(\gamma-1)/\gamma} = (M_{-\infty}A)^2$$

$$= 1 - \frac{\gamma-1}{2} M_{-\infty}^2 \left[(\nabla\Phi)^2 - 1\right] = \frac{1 + (\gamma-1)M_{-\infty}^2/2}{1 + (\gamma-1)M^2/2} \tag{16}$$

applies in continuous regions of the steady field. In addition, the flow remains attached at blade surfaces; i.e.,

$$\nabla\Phi \cdot \vec{n} = 0 , \quad \text{on } B_m \tag{17}$$

and mass and tangential momentum are conserved across shocks; i.e.,

$$\left[\!\left[\bar{\rho}\nabla\Phi\right]\!\right]\cdot\vec{n}=0 \quad , \qquad \text{on } Sh_{m,\pm} \tag{18}$$

and

$$\left[\!\left[\Phi\right]\!\right]_{\tau}=\left[\!\left[\Phi\right]\!\right]=0, \qquad \text{on } Sh_{m,\pm} \tag{19}$$

Wake jump conditions are automatically satisfied in the two-dimensional steady problem since the zeroth-order flow is continuous downstream of the blade row. Finally, steady subsonic velocities are uniform far upstream and downstream of the blade row; i.e.,

$$\nabla\Phi=\vec{V}_{\mp} \quad , \qquad \xi\rightarrow\mp\infty \tag{20}$$

where ξ is the axial coordinate in Fig. 1. In general, the inlet Mach number and flow direction are prescribed along with either the exit flow direction or the imposition of a Kutta condition at blade trailing edges. The exit Mach number is then determined by a global mass balance.

The Linear Unsteady Problem

It follows from the potential, Eq. (1) and Bernoulli, Eq. (2), equations and the asymptotic expansions for the flow variables (e.g., Eq. (10)) that the linear unsteady flow is governed by the conservative form differential equation

$$\frac{\partial\rho}{\partial t}+\nabla\cdot\left[\bar{\rho}\nabla\phi+\rho\nabla\Phi\right]=0 \tag{21}$$

and the unsteady density, ρ, pressure, p, and speed of sound, a, are related by

$$\rho/\bar{\rho}=\gamma^{-1}\,p/P=\left(\frac{2}{\gamma-1}\right)a/A=-A^{-2}\frac{D_S\phi}{Dt} \tag{22}$$

where $\dfrac{D_S}{Dt}$ is a mean-flow convective derivative operator; i.e.,

$$\frac{D_S}{Dt}=\frac{\partial}{\partial t}+\nabla\Phi\cdot\nabla=i\omega+\nabla\Phi\cdot\nabla \tag{23}$$

Upon substituting the steady, Eq. (16), and unsteady, Eq. (22), Bernoulli relations into Eq. (21); or alternatively, the series expansion, Eq. (10), into the time-dependent potential equation, Eq. (3), and performing some algebra, the following

nonconservative differential equation for the unsteady potential is obtained

$$A^2 \nabla^2 \phi = \frac{D_s^2 \phi}{Dt^2} + (\gamma-1) \nabla^2 \Phi \frac{D_s \phi}{Dt} + \nabla(\nabla \Phi)^2 \cdot \nabla \phi / 2 \qquad (24)$$

or

$$A^2 \nabla^2 \phi - \nabla \Phi \cdot \left[(\nabla \Phi \cdot \nabla) \nabla \phi \right]$$

$$- \left[\left[2i\omega + (\gamma-1) \nabla^2 \Phi \right] \nabla \Phi + \nabla(\nabla \Phi)^2 \right] \cdot \nabla \phi \qquad (25)$$

$$+ \left[\omega^2 - i\omega(\gamma-1) \nabla^2 \Phi \right] \phi = 0$$

The principal part of the unsteady differential equation is given by the first two terms in Eq. (25).

Surface Conditions

Similarly, conditions on the unsteady flow at blade, wake, and shock mean positions are obtained by substituting the asymptotic and Taylor, Eq. (11), series expansions and the surface vector relations, Eq. (12), into the time-dependent flow tangency, Eq. (4), wake-continuity, Eq. (7), and shock-jump, Eqs. (8) and (9), conditions. After a substantial amount of straightforward algebra and the application of the steady surface conditions, Eqs. (17) through (19), the following conditions on the linear unsteady flow are determined. The first-order flow tangency condition has the form

$$\nabla \phi \cdot \vec{n} = \left[i\omega \vec{r} + (\nabla \Phi \cdot \vec{\tau})(\vec{\tau} \cdot \nabla)\vec{r} - (\vec{r} \cdot \nabla) \nabla \Phi \right] \cdot \vec{n} e^{im\sigma}, \qquad \text{on } B_m \qquad (26)$$

For rigid blade motions, this reduces to

$$\nabla \phi \cdot n = \left[i\omega \vec{r} + \vec{\alpha} \times \nabla \Phi - (\vec{r} \cdot \nabla) \nabla \Phi \right] \cdot \vec{n} e^{im\sigma}$$

$$= \left[i\omega \vec{r} - \nabla(\vec{r} \cdot \nabla \Phi) \right] \cdot \vec{n} e^{im\sigma}, \qquad \text{on } B_m \qquad (27)$$

The first term on the right hand side of Eq. (27) is the velocity of the blade motion. The second term accounts for the effects of blade rotation relative to the mean flow and of motion through a spatially varying mean velocity field. Since the steady flow is continuous downstream of the blade row, the conditions of continuity of normal velocity and pressure across blade wakes (c.f. Eq. (7)) reduce to

$$[\![\nabla \phi]\!] \cdot \vec{n} = \left[\!\!\left[\frac{D_s \phi}{Dt} \right]\!\!\right] = 0, \qquad \text{on } W_m \qquad (28)$$

where the mean positions, W_m, of the unsteady wakes are assumed to coincide with the downstream, steady-flow, stagnation streamlines.

For shocks with negligible curvature, conservation of mass and tangential momentum require that

$$-\left[i\omega r + \Phi_\tau \frac{\partial r}{\partial \tau}\right] e^{im\sigma} [\![\bar{p}]\!] + [\![\bar{\rho}\nabla\phi + \rho\nabla\Phi]\!] \cdot \vec{n}$$
$$+ re^{im\sigma} \frac{\partial}{\partial n} [\![\bar{\rho}\Phi_n]\!] = 0 \quad, \qquad \text{on } Sh_{m,\pm} \tag{29}$$

and

$$\frac{\partial}{\partial\tau}\left[[\![\phi]\!] + e^{im\sigma} r[\![\Phi_n]\!]\right] = [\![\phi]\!] + e^{im\sigma} r[\![\Phi_n]\!] = 0 \ , \qquad \text{on } Sh_{m,\pm} \tag{30}$$

respectively, where $\vec{\Re} \cdot \vec{n} = re^{i(\omega t + m\sigma)}$ is the shock displacement in the direction normal to the shock. Conditions (29) and (30) provide two relations for determining the jump in the unsteady potential across the shock and the shock displacement. For normal shocks, i.e., $\Phi_\tau|_{Sh} = 0$, it follows from the zeroth-order continuity equation, Eq. (1), that $\frac{\partial}{\partial n}[\![\bar{\rho}\Phi_n]\!] = 0$, and therefore

$$[\![\bar{\rho}\phi_n + \rho\Phi_n]\!] = i\omega re^{im\sigma}[\![\bar{p}]\!] = -i\omega[\![\bar{p}]\!][\![\phi]\!]/[\![\Phi_n]\!], \qquad \text{on } Sh_{m,\pm} \tag{31}$$

After substituting the first-order Bernoulli equation, Eq. (22), into Eq. (31), the following implicit expression for the jump in the unsteady potential across the shock is obtained

$$i\omega[\![\bar{p}]\!][\![\phi]\!] = [\![\Phi_n]\!]\left\{\bar{\rho}\Phi_n M_{-\infty}^2\left[i\omega[\![\phi/\bar{\rho}^{(\gamma-1)}]\!]\right]\right.$$
$$\left. + (\bar{\rho}\Phi_n)[\![\phi_n/\bar{\rho}^\gamma]\!]\right] - [\![\bar{\rho}\Phi_n]\!]\right\} \quad, \qquad \text{on } Sh_{m,\pm} \tag{32}$$

where the $\bar{\rho}$ and Φ are known from the steady solution.

Unsteady Far-Field Solutions

To complete the specification of the unsteady boundary value problem, conditions far upstream and downstream of the blade row must be established. In general, unsteady disturbances do not attenuate far from the blade row, and hence, it is difficult to place explicit far-field conditions on the unsteady potential. Instead, analytic far-field solutions to the unsteady differential equation, Eq. (24), have been determined for uniform subsonic inlet and exit conditions. These analytic solutions can be matched to a near-field numerical solution at finite distances

upstream and downstream from the blade row (e.g., at $\xi = \xi_{\mp}$ in Fig. 2). It is assumed that for $\xi < \xi_-$ and $\xi > \xi_+$, the departure of steady flow quantities from their free-stream values is of $\mathcal{O}(\epsilon)$; e.g.,

$$\left| \vec{V}(\xi) - \vec{V}_{\mp\infty} \right| \sim \mathcal{O}(\epsilon) \qquad \mp \xi > \left| \xi_{\mp} \right| \tag{33}$$

The unsteady potential is continuous far upstream of the blade row (i.e., $\phi = \phi_c$ for $\xi < \xi_-$) and has both continuous and discontinuous components downstream of the blade row (i.e., $\phi = \phi_c + \phi_d$ for $\xi > \xi_+$). The continuous potential accounts for acoustic wave propagation into the far-field. Fourier methods can be used to provide expressions for this component of the far-field potential in terms of the cascade axial and tangential coordinates ξ and η (Fig. 2). It follows that (c.f., Refs. 17 and 31)

$$\phi_c(\xi,\eta) = \sum_{j=-\infty}^{\infty} b_{j,\mp} \exp(iq_j\eta)\exp\left[\chi_{j,\mp}(\xi - \xi_{\mp})\right], \qquad \mp\xi \ge \left| \xi_{\mp} \right| \tag{34}$$

where the coefficients, $b_{j,\mp}$, are obtained from the relation

$$b_{j,\mp} = G^{-1} \int_{\eta}^{\eta + G} \phi_c(\xi,\eta)\exp(-iq_j\eta)\,d\eta, \qquad \xi = \xi_{\mp} \tag{35}$$

The discontinuous component of the unsteady potential far downstream results from the counter vorticity shed from the trailing edges of the blades and convected along the blade wakes. A closed form solution (Refs. 17, 31) for this potential has been determined and is given by

$$\phi_d(\tau,n) = \Delta\phi(\xi_+,\eta_+)\, F(n)\exp(-i\omega\tau/V_\infty), \qquad \xi \ge \xi_+ \tag{36}$$

where τ and n are Cartesian coordinates with the τ-axis coinciding with the far-downstream, zeroth wake (Fig. 2). The constants q_j, $\chi_{j,\mp}$ and the function $F(n)$ in the foregoing equations are defined explicitly in Ref. 17.

Aerodynamic Response Coefficients

Solutions to the steady and unsteady boundary value problems are required to determine blade pressure distributions and aerodynamic force and moment coefficients. The pressure at the mth blade surface is given by (c.f. Eq. (14))

$$P_{\mathcal{B}_m} = P_{\mathcal{B}} + P_{\mathcal{B}}\, e^{i(\omega t + m\sigma)} + \mathcal{O}(\epsilon^2) \tag{37}$$

where P and $pe^{i\omega t}$ are the zeroth-(steady) and first-(unsteady) order components of the fluid pressure, and ℬ and B denote the moving and mean reference blade surfaces, respectively. After expanding the pressure $\hat{P}(\hat{\vec{X}}, t)$, in the manner indicated by Eqs. (10) and (11), it follows from the steady and unsteady Bernoulli equations that

$$P_B = 2(\gamma M_{-\infty}^2)^{-1} (M_{-\infty} A)_B^{2\gamma/(\gamma-1)} \qquad (38)$$

and

$$
\begin{aligned}
p_\circledast &= \left[-2(M_{-\infty} A)^{2/(\gamma-1)} \frac{D_s \phi}{Dt} + (\vec{r} \cdot \nabla) P \right]_B \\
&= -2(M_{-\infty} A)^{2/(\gamma-1)} \left[\frac{D_s \phi}{Dt} + (\vec{r} \cdot \nabla)(\nabla \Phi)^2/2 \right]_B
\end{aligned}
\qquad (39)
$$

Thus the steady and unsteady components of the pressure acting on a moving blade surface, $\circledast_m$, are evaluated in terms of information supplied at the mean position of the reference blade, B. The first term of the right-hand-side of Eq. (39) is the unsteady pressure at the mean position of the blade and the second is due to motion through a spatially varying steady pressure field.

The force and moment coefficients acting on the mth blade; i.e.,

$$\hat{\vec{C}}_{F_m} = \vec{C}_F + \vec{c}_F \, e^{i(\omega t + m\sigma)} + \mathcal{O}(\epsilon^2) \qquad (40)$$

and

$$\hat{C}_{M_m} = C_M + c_M \, e^{i(\omega t + m\sigma)} + \mathcal{O}(\epsilon^2) \qquad (41)$$

are determined by simple integrations over the mean position of the reference blade. After some algebra it follows that the steady, $\vec{C}_F$ and C_M, and, for rigid blade motions, the unsteady, $\vec{c}_F$ and c_M, force and moment coefficients are given by

$$\vec{C}_F = - \oint_B P_B \vec{n} \, d\tau \, , \qquad C_M = \oint_B P_B \vec{R}_P \cdot d\vec{\tau} \qquad (42)$$

and

$$c_F = - \oint_B p_\circledast \vec{n} \, d\tau + \alpha \times \vec{C}_F, \qquad c_M = \oint_B p_\circledast \vec{R}_P \cdot d\vec{\tau} \qquad (43)$$

where $d\vec{\tau}$ is a differential vector tangent to the mean blade surface. It should be noted that the moment is taken about the moving pitching axis. The unsteady force

and moment coefficients are the important results of an aerodynamic analysis intended for bending or torsional flutter predictions. Knowledge of these coefficients permits the evaluation of aerodynamic work per cycle and/or aerodynamic damping (Ref. 32) either of which can be used to determine whether the airstream supports or suppresses a prescribed blade motion.

THE UNSTEADY NUMERICAL SOLUTION PROCEDURE

The solution procedure will be outlined for flow past a cascade of sharp-edged airfoils with mean positions aligned with the steady flow. Thus unsteady phenomena associated with leading edge bluntness, mean incidence, and mean flow stagnation (c.f. Refs. 23 and 24) are omitted from present consideration so that attention can be focused on the transonic aspects (i.e., local supersonic regions and shock discontinuities) of the unsteady problem. A numerical resolution of the linear, variable-coefficient, unsteady, boundary-value problem is required over a single, extended, blade-passage region of finite extent (Fig. 2). The unsteady differential equation must be solved in continuous flow regions subject to boundary or jump conditions at the mean positions of the blade, wake and shock surfaces. Blade mean positions are prescribed, and the mean position of wake (i.e., the downstream stagnation streamlines) and shock surfaces are determined as part of the steady flow solution. Finally, the near-field numerical solution must be matched to far-field analytical solutions at finite distances ($\xi = \xi_{\mp}$) upstream and downstream from the blade row to account for acoustic wave propagation into the far-field and vorticity convection along the far-downstream blade wakes.

For the numerical resolution of the unsteady transonic problem various components must be selected or constructed. These include the computational coordinate system, the discrete domain (or calculation mesh), differencing strategies for mixed flows, the approximating algebraic equations, and the solution procedure. These components are generally not independent of each other and it is important that the choice of one does not place overly restrictive constraints on the others.

Coordinate System and Calculation Mesh

The coordinate system selected for the present study is the ξ, η-Cartesian system where the ξ and η-coordinate axes are directed along the cascade axial and circumferential directions, respectively (Fig. 1). For sharp-edged blades the origin of this system coincides with the leading edge of the reference blade (i.e., m = 0). For Cartesian independent variables, in this case ξ and η, the unsteady differential equation, (Eq. 24), can be written in the form

$$\mathscr{L}_0 \phi = \sum_{\nu=0}^{5} c^{\nu} \mathcal{D}_{\nu} \phi = 0 \qquad (44)$$

where the linear differential operators $\mathcal{D}_{\nu}$ are defined by

$$\mathcal{D}_0 \phi = \phi \qquad \mathcal{D}_1 \phi = \phi_{\xi} \qquad \mathcal{D}_2 \phi = \phi_{\eta}$$

$$(45)$$

$$\mathcal{D}_3 \phi = \phi_{\xi\xi} \qquad \mathcal{D}_4 \phi = \phi_{\xi\eta} \qquad \mathcal{D}_5 \phi = \phi_{\eta\eta}$$

and the variable coefficients C^ν depend on the underlying steady flow; i.e.,

$$C^0 = \omega^2 - i\omega(\gamma-1)\nabla^2\Phi$$

$$C^1 = -\left[2i\omega + (\gamma-1)\nabla^2\Phi\right]\Phi_\xi - 2\nabla\Phi\cdot\nabla\Phi_\xi$$

$$C^2 = -\left[2i\omega + (\gamma-1)\nabla^2\Phi\right]\Phi_\eta$$

$$C^3 = A^2 - \Phi_\xi^2 \qquad C^4 = -2\Phi_\xi\Phi_\eta \qquad C^5 = A^2 - \Phi_\eta^2$$

(46)

Cascade flows place stringent requirements on computational grids. In particular, it is desirable to have grid lines parallel and normal to solid surfaces and surfaces of discontinuity so that boundary and jump conditions can be implemented accurately. Moreover, the mesh should be periodic to facilitate the implementation of cascade periodicity conditions and, for unsteady flows, one set of far-field mesh lines should be parallel to the blade row to facilitate the matching of analytical far-field and numerical near-field solutions. Further, it should be possible to con-centrate mesh points at the appropriate density in critical regions of the flow, such as near blade surfaces and shocks, and near blade leading and trailing edges. Finally, the mesh should not be highly sheared and mesh aspect ratios should not depart too far from one, as this tends to degrade solution accuracy and, in some cases, lead to numerical stability problems. It is usually not possible to obtain a grid which meets all of the foregoing requirements and, as a result, some compromises have to be made (c.f. Ref. 21).

In the present study the basic approach is to capture large scale unsteady phenomena on a rectilinear-type (cascade) mesh of moderate density which covers an extended blade-passage region, and then to match the cascade solution to local solutions determined on dense grids covering limited regions of high velocity gradient; for example, near a rounded blade leading edge (Refs. 23, 24) and near shocks. To date, our unsteady transonic calculation procedure has only been imple-mented on the cascade mesh, but work is currently proceeding on the development of a local unsteady calculation for the resolution of shock phenomena. The cascade mesh used here is the periodic and body-fitted, but nonorthogonal, one shown schematically in Fig. 3. It is composed of axial lines (ξ = constant), which are parallel to the blade row making the mesh periodic, and "tangential" curves which are percentile averages of the upper and lower boundaries making the mesh body fitted. This mesh facilitates the implementation of blade and wake boundary conditions as well as cascade periodicity conditions and the matching of analytical and numerical unsteady solutions in the far-field. However, the unsteady flow in the vicinity of rounded blade edges or in the vicinity of shocks cannot be accurately resolved.

Differencing Strategies for Transonic Flow

Following the ideas of Murman and Cole (Refs. 27, 28), the plan is to distinguish between regions of subsonic flow where the governing differential equation is ellip-tic, sonic flow where it is parabolic, and supersonic flow where it is hyperbolic,

and to use a difference scheme which is sensitive to the local character of the unsteady differential equation. To accomplish this we first apply the rotated differencing concept introduced by Jameson (Ref. 26). At each point of the discrete domain the unsteady equation is expressed in canonical form; i.e.,

$$\mathcal{L}_0\phi = (\mathcal{L}_1 + \mathcal{L}_2)\phi \tag{47}$$

where

$$\mathcal{L}_1\phi = A^2(1-M^2)\phi_{SS} \tag{48}$$

$$\mathcal{L}_2\phi = A^2\phi_{NN} + \cdots$$

and S and N are local Cartesian coordinates aligned with and normal to, respectively the local steady flow direction. In Eqs. (47) and (48) the principal part of the unsteady differential equation is shown explicitly and the dots refer to the remaining terms (which are left in their original form). It is now clear that the local type of the unsteady equation depends on the local Mach number of the steady flow. Since the ξ, η-coordinates at a given point Q are related to the canonical coordinates at this point by the transformation

$$\xi = \left|\nabla\Phi\right|^{-1}(\Phi_\xi S - \Phi_\eta N) + \vec{X}_\xi(Q)$$

$$\eta = \left|\nabla\Phi\right|^{-1}(\Phi_\eta S + \Phi_\xi N) + \vec{X}_\eta(Q) \tag{49}$$

$\mathcal{L}_1$ and $\mathcal{L}_2$ can be expressed in the following equivalent forms

$$\mathcal{L}_1\phi = A^2(1-M^2)\phi_{SS} = \frac{(1-M^2)}{M^2}(\Phi_\xi^2\phi_{\xi\xi} + 2\Phi_\xi\Phi_\eta\phi_{\xi\eta} + \Phi_\eta^2\phi_{\eta\eta})$$

$$\mathcal{L}_2\phi = A^2\phi_{NN} + \cdots \tag{50}$$

$$= \frac{1}{M^2}\left[\Phi_\eta^2\phi_{\xi\xi} - 2\Phi_\xi\Phi_\eta\phi_{\xi\eta} + \Phi_\xi^2\phi_{\eta\eta}\right] + \cdots$$

It is now a simple matter to construct a suitable type-dependent differencing scheme. The linear operator $\mathcal{L}_2$ is always approximated by central difference expressions, but the difference approximation to the operator $\mathcal{L}_1$ will depend on the local steady Mach number and hence, the local type of unsteady differential equation. Thus if $M_{i-1,j}$ and $M_{i,j}$ are both less than one, where i and j are grid point indices for the axial and tangential mesh lines, respectively, the flow is locally subsonic (elliptic) and

$$\underline{M_{i,j} < 1 \ , \ M_{i-1,j} < 1}$$

$$\mathcal{L}_1\phi\Big|_{i,j} \approx L_1\phi\Big|_{i,j} \tag{51}$$

where L is a central difference operator. If $M_{i-1,j} < 1$ and $M_{i,j} > 1$, the flow is accelerating through sonic velocity (parabolic) at the point (i,j) and $\mathcal{L}_1\phi$ is set equal to zero; i.e.,

$$\underline{M_{i-1,j} < 1, M_{i,j} > 1}$$

$$\mathcal{L}_1\phi \approx 0 \qquad (52)$$

If $M_{i-1,j} > 1$ and $M_{i,j} > 1$, the flow is locally supersonic (hyperbolic) at (i,j) and $\mathcal{L}_1\phi$ is approximated by a retarded or upwinded difference expression

$$\underline{M_{i,j-1} > 1, \qquad M_{i,j} > 1}$$

$$\mathcal{L}_1\phi\Big|_{i,j} \approx L_1\phi\Big|_{i-1,j} \qquad (53)$$

i.e., a central difference expression evaluated at the previous upstream point on the jth tangential mesh line. Strictly speaking, at supersonic points the differencing should be retarded along both tangential and axial mesh lines, but since the tangential mesh lines are closely aligned with the flow direction (except at rounded blade edges), it should be sufficient to upwind difference only along tangential mesh lines. Finally if $M_{i-1,j} > 1$ and $M_{i,j} < 1$, there are two possibilities: a) if a shock is to be fitted into the unsteady solution, shock-jump conditions are imposed at the point (i,j) with one-sided difference expressions used to approximate normal (to the shock) derivatives of the unsteady potential on either side of the shock, and (b) if no shock occurs or if unsteady shock phenomena are to be captured; i.e., the differential equation is solved through the shock, than subsonic differencing, Eq. (51), is applied at the point (i,j). Thus

$$\underline{M_{i-1,j} > 1, \quad M_{i,j} < 1}$$

(a) shock fitting

(b) $\mathcal{L}_1\phi\Big|_{i,j} \approx L_1\phi\Big|_{i,j}$ $\qquad (54)$

Algebraic Approximations

Finite difference approximations to the various linear operators appearing in the unsteady boundary value problem are determined using an implicit, least-squares interpolation which is applicable on arbitrary grids. Consider a linear differential operator $\mathcal{L}$ which operates on a constant by multiplying that constant by q^0. $\mathcal{L}\phi$ is to be approximated at the mesh point Q_0 in terms of the values of ϕ at Q_0 and at certain neighboring mesh points, Q_1, ..., Q_M, which, with Q_0 are called a neighbor set. Neighbor sets are defined as shown in Fig. 3, i.e., in a "centered" fashion for interior points of the solution domain and in a "one-sided" fashion for points on a blade, wake or shock surface. Quantities subscripted with 0 or m are evaluated at the corresponding neighbor set member. The approximation is developed in terms of an implicit interpolation of the form

23

$$\delta\phi \equiv \phi - \phi_0 \approx F = \sum_{n=1}^{N} \gamma^n f^n \equiv \underset{\sim}{f}^T \underset{\sim}{\gamma} \tag{55}$$

where the f^n are prescribed interpolating functions which vanish at Q_0 (homogeneous polynomials, for instance) and the γ^n are interpolating coefficients which depend on local values of ϕ and are determined by the specific interpolation used. An algebraic approximation to $(\mathscr{L}\phi)_0 = \phi(Q_0)$ is then simply obtained by replacing ϕ with $\phi_0 + F$, i.e.,

$$(\mathscr{L}\phi)_0 \approx \mathscr{L}(\phi_0 + F)_0 = q^0\phi_0 + (\underset{\sim}{\mathscr{L}f})_0^T \underset{\sim}{\gamma} \tag{56}$$

where $\mathscr{L}f$ is the $N \times 1$ vector with components $\mathscr{L}f^n$.

For the present application the interpolating functions are chosen to be the polynomials

$$N = 5: \quad f^1 = \delta\xi, \quad f^2 = \delta\eta, \quad f^3 = \delta\xi^2, \quad f^4 = \delta\xi \cdot \delta\eta, \quad f^5 = \delta\eta^2 \tag{57}$$

where $\delta\xi = \xi - \xi_0, \delta\xi^2 = (\xi-\xi_0)^2$ etc. The interpolating coefficients must then be identified. With eight neighbors but only five interpolating functions, it is impossible to define γ such that F implicitly agrees with $\delta\phi$ at all neighbors. Least-squares techniques provide a formal method for defining the interpolating coefficients from the available data regardless of the geometry of the neighbor set.

A measure of the error in replacing $\delta\phi$ with its interpolate F in Eq. (55) is

$$e(\underset{\sim}{\gamma}) \equiv \sum_{m=1}^{M} W_m \left[\sum_{n=1}^{N} \gamma^n f_m^n - \delta\phi_m \right] \overline{\left[\sum_{n=1}^{N} \gamma^n f_m^n - \delta\phi_m \right]} \tag{58}$$

where the overbar indicates complex conjugation and the W_m are chosen to give proper importance to the various neighbors. In practice W_m is usually given by

$$W_m = 1 / |Q_m - Q_0| \tag{59}$$

but it may be set to zero if the corresponding neighbor is to have no influence. Note that since ϕ is complex and the f^n are real, the γ^n must be complex. The error function is minimized by setting its derivatives with respect to the real and imaginary parts of the γ^n equal to zero. There results the complex linear system

$$\sum_{n=1}^{N} \left(\sum_{m=1}^{M} W_m f_m^n \bar{f}_m^k \right) \gamma^n = \sum_{m=1}^{M} W_m \bar{f}_m^k \delta\phi_m; \quad k = 1, \dots, N \tag{60}$$

24

which can be written in compact form as

$$\mathbf{Q}\underset{\sim}{\gamma} = \mathbf{B}\underline{\delta\phi} \tag{61}$$

The $N \times N$ matrix $\mathbf{Q}$ and the $N \times M$ matrix $\mathbf{B}$ are given in terms of the $M \times N$ matrix $\mathbf{F} = (f_m^k)$ and the $M \times M$ diagonal matrix, $W = \text{diagonal}(W_1, \ldots, W_m)$ by

$$\mathbf{Q} = \mathbf{F}^* W \mathbf{F} \qquad \mathbf{B} = \mathbf{F}^* W \tag{62}$$

where the superscript $*$ indicates conjugate transposition. Thus

$$\underset{\sim}{\gamma} = (\mathbf{Q}^{-1}\mathbf{B})\underline{\delta\phi} = C\underline{\delta\phi} \tag{63}$$

where C is an $N \times M$ matrix. By combining Eqs. (56) and (63) the approximating difference operator can be defined in terms of the local values of ϕ by

$$(\mathcal{L}\phi)_0 \approx (L\phi)_0 \equiv q^0 \phi_0 + (\underline{\mathcal{L}f})_0^T C\underline{\delta\phi}$$
$$= q^0 \phi_0 + \sum_{m=1}^{M} \beta_m (\phi_m - \phi_0) \tag{64}$$

where the difference coefficients, β_m, are given by

$$\underset{\sim}{\beta}^T = (\beta_1, \ldots, \beta_M) \equiv (\underline{\mathcal{L}f})_0^T C \tag{65}$$

The foregoing difference approximation is flexible enough so that neighbor sets can be adjusted to avoid differencing across singularities -- an important feature for the linear unsteady problem -- and across shocks. In addition, both differential equation and surface conditions can be simultaneously approximated at surface points. The latter strategy can significantly improve the diagonal dominance of the resulting set of algebraic equations and the accuracy of the calculation in regions where mesh aspect ratios are abnormally large or small. The reader is referred to Refs. 22 and 23 for further details on this algebraic difference approximation.

<center>Solution Procedure</center>

At field points the unsteady differential equation, Eq. (44), is approximated using centered neighbor sets (Fig. 3) along with the type-dependent differencing strategies of Eqs. (51) through (54). For points on the upstream periodic boundary, ϕ values at neighbors above the mesh region are related to ϕ values at points within the mesh region by the periodic condition, Eq. (14). On the lower periodic boundary

the periodic condition is applied directly, since to approximate the field equation on both upper and lower periodic boundaries would be redundant. For points on the far-upstream or far-downstream boundaries ($\xi = \xi_{\mp}$ in Fig. 2) ϕ values at neighbors upstream or downstream, respectively, are related to ϕ values on the boundaries using the far-field analytic solutions, Eqs. (34) and (36), with the Fourier coefficients being evaluated using Eq. (35). The infinite sum in Eq. (34) is truncated after a few terms – usually three – in each direction, and the integral in Eq. (35) is approximated using trapezoid rule quadrature. At blade and wake points the flow tangency condition, Eq. (26), and the wake continuity conditions, Eq. (28), are approximated, respectively, using one-sided neighbor sets. At both blade and wake points, the difference equations can be constrained so that the field equation is also satisfied (c.f. Ref. 22). Finally, when shocks are fitted into the unsteady solution, the shock-jump conditions, Eqs. (29) and (30), or for normal shocks, Eq. (32), are imposed using first-order accurate, one-sided differences to approximate derivatives normal to the shock.

Let ϕ_i be a vector of ϕ values on the ith axial mesh line. Because: (1) neighbor sets of points on the ith line include only points from lines i-1, i, and i+1; (2) the algebraic approximation to the unsteady differential equation involves only neighbor sets centered on the lines i and i-1; (3) first-order accurate difference approximations are used to fit shocks; and (4) the cascade mesh is periodic; the system of linear algebraic equations, which approximate the unsteady boundary value problem, have the following block quadridiagonal form.

$$
\begin{aligned}
C_1 \underset{\sim}{\phi}_1 + D_1 \underset{\sim}{\phi}_2 &= \underset{\sim}{F}_1 \\
A_i \underset{\sim}{\phi}_{i-2} + B_i \underset{\sim}{\phi}_{i-1} + C_i \underset{\sim}{\phi}_i + D_i \underset{\sim}{\phi}_{i+1} &= \underset{\sim}{F}_i \qquad 2 \le i \le I-1 \\
B_I \underset{\sim}{\phi}_{i-1} + C_I \underset{\sim}{\phi}_I &= \underset{\sim}{F}_I
\end{aligned}
\tag{66}
$$

Note that $A_i \equiv 0$ at subsonic (and at sonic) points, except when the ith axial mesh line is immediately downstream of a fitted shock. With this structure the system can be solved directly and efficiently using Gaussian elimination. The submatrices A_i, B_i, C_i and D_i are sparse being basically scalar tridiagonal. This feature can be taken advantage of to improve computational efficiency during the forward elimination phase of the solution (Ref. 33).

NUMERICAL RESULTS

The foregoing analysis has been applied to determine unsteady subsonic and transonic flows past vibrating cascades of sharp-edged, double-circular-arc (DCA) airfoils with blade mean positions aligned with the steady flow. The zeroth or reference blade surface is defined by the equation

$$y_{\pm}(x) = \text{sgn}(H_{\pm}) \left[|H_{\pm}| - R_{\pm} + \sqrt{R_{\pm}^2 - (x - 0.5)^2} \right], \qquad H_{\pm} \neq 0$$

$$= 0, \qquad H_{\pm} = 0 \tag{67}$$

where H is the y-coordinate of the surface at midchord, R is the radius of curvature; i.e.,

$$R = (H^2 + 0.25)/2|H| \tag{68}$$

sgn (y) = ± 1 for H ⪌ 0, and the subscripts + and − refer to the upper (suction) and lower (pressure) surfaces of the blade. For purposes of comparison, subsonic flows past vibrating flat plate (H = 0) cascades have also been calculated. In this case $\Phi = x$ and the unsteady equations reduce to those of classical linear theory.

In this report unstaggered ($\Theta = 0$ deg.) and staggered (with $\Theta = 45$ deg.) cascades with unit gap/chord ratio (G = 1) of 5% thick, flat-bottomed, DCA ($H_+ = 0.05$, $H_- = 0$) and flat plate blades are considered. Unsteady surface pressure ($p_{\circledB}$) and pressure difference (Δp) distributions, where

$$\Delta p(x) = p_{\circledB -}(\vec{X}) - p_{\circledB +}(\vec{X}) = p_{\circledB_i}(\vec{X} + \vec{G})e^{-i\sigma} - p_{\circledB_0 +}(\vec{X}) \tag{69}$$

and aerodynamic lift ($c_L = \vec{c}_F \cdot \vec{e}_y$) and moment ($c_M$) coefficients will be presented for blades undergoing out-of-phase ($\sigma = 180$ deg.), single-degree-of-freedom bending (with $h_y = (1, 0)$) or torsional (with $\alpha = (1, 0)$) vibrations at prescribed frequencies (ω) and inlet Mach numbers ($M_{-\infty}$). Corresponding exit Mach numbers (M_∞) and inlet ($\Omega_{-\infty}$) and exit (Ω_∞) flow angles are determined, as part of the steady flow calculation, from a global mass balance and the application of a Kutta condition; i.e.,

$$\vec{V} \cdot d\vec{\tau} \Big|_{B-} = - \vec{V} \cdot d\vec{\tau} \Big|_{B+}, \qquad x = 0, 1 \tag{70}$$

at blade leading and trailing edges. When the imaginary parts of the bending or torsional amplitudes are set equal to zero, the real and imaginary parts of the response coefficients are in phase with blade displacement and velocity, respectively. Further, the stability of single-degree-of-freedom bending or torsional motions is governed by the sign of the imaginary part of the lift or moment coefficients, respectively. If $Im\{c_L\} < 0$ for bending or $Im\{c_M\} < 0$ for torsion, the airstream tends to suppress the motion, and hence, this motion is stable according to linear theory (Ref. 34).

Steady Mach Number Distributions

Full potential steady flows have been determined using the finite-area numerical approximation developed by Caspar, Hobbs, and Davis (Ref. 35) for subsonic cascade flows, and subsequently extended by Caspar (Ref. 36) for transonic flows. A steady transonic solution is first determined on a cascade mesh (Fig. 3), and then the cascade mesh solution is matched to a local solution determined on a dense mesh (Fig. 4) which covers and extends well beyond the supersonic region. The solution to the steady boundary value problem is taken to be the local solution in the region covered by the local mesh and the cascade solution elsewhere. It should be noted that with the numerical procedure of Refs. 35 and 36, the steady differential equation is solved in conservative form and shocks are captured. However, due to the fine resolution possible with the local mesh, it appears that steady information upstream and downstream of the shock can be determined with sufficient accuracy to fit shocks into the unsteady solution.

Surface Mach number distributions for the unstaggered and staggered DCA cascades are shown in Figs. 5 and 6, respectively. For the unstaggered case the prescribed inlet (and calculated exit) Mach numbers are 0.70, 0.72, 0.74, and 0.76. Corresponding inlet and exit flow angles vary from $\Omega_{\mp\infty} = \pm 4.3$ deg. for $M_{-\infty} = 0.70$ to $\Omega_{\mp\infty} = \pm 4.65$ deg. for $M_{-\infty} = 0.76$. At the lower Mach numbers, $M_{-\infty} = 0.7$, $M_{-\infty} = 0.72$, and $M_{-\infty} = 0.74$, the steady flows are continuous with peak Mach numbers of .91, .95, and 1.01, respectively, occurring at midchord on the blade suction surface. For $M_{-\infty} = 0.74$ a supersonic region extends from 43% chord to 57% chord along the suction surface. At the highest inlet Mach number, $M_{-\infty} = 0.76$, a shock impinges on the blade suction surface at a distance of 64% of blade chord from the leading edge. The Mach number on the upstream and downstream sides of the shock are 1.157 and 0.935, respectively, and the supersonic region extends from 32% of chord to 64% of chord on the blade suction surface.

For the 45 deg. staggered DCA cascade (Fig. 6) the prescribed inlet Mach numbers are 0.8, 0.85, and 0.9. The corresponding exit Mach numbers and inlet flow angles are 0.62, 0.64, and 0.65, and 4.4 deg., 4.5 deg., and 4.6 deg., respectively. The exit flow angle is -2.0 deg. in each case. Continuous steady flows occur at $M_{-\infty} = 0.8$ and $M_{-\infty} = 0.85$ with peak suction-surface Mach numbers of 0.94 and 1.033 occurring at 32% and 30% of blade chord, respectively, downstream of the leading

edge. At $M_{-\infty} = 0.85$ the flow is supersonic along the suction surface from 22% to 42% of chord. For $M_{-\infty} = 0.9$ the steady flow is discontinuous with the supersonic region adjacent to the blade suction surface extending from 20% to 47% of blade chord and terminating at a shock. Mach numbers just upstream and downstream of the shock are 1.19 and 0.87, respectively.

Unsteady Solution Behavior

Unsteady solutions for the DCA and flat plate cascades have been determined on a cascade mesh extending two axial chords upstream and downstream of the blade row. The mesh consists of 15 tangential and from 75 to 81 axial lines, 31 to 37 of which intersect blade surfaces. A variable mesh spacing is used with tangential mesh lines concentrated near blade and wake surfaces and axial mesh lines concentrated near blade edges and shocks as well as in supersonic regions. Steady data, determined on a similar but much coarser cascade mesh and on a dense local mesh (Fig. 4), are defined on the unsteady mesh using constrained, polynomial, least-squares interpolations in an explicit manner.

Before proceding with the unsteady parametric studies, it is of interest to illustrate several features of the unsteady numerical approximation. The reference flow for this discussion is that past an unstaggered cascade of 5% thick, flat-bottomed, DCA airfoils undergoing low-frequency ($\omega = 0.1$) torsional oscillations at an inlet Mach number of 0.76. The steady Mach number distribution on the reference blade surface is shown in Fig. 5. To assess the impact of the type-dependent and rotated differencing schemes, unsteady response predictions have been determined first by using these strategies along with shock capturing, and then by using subsonic or central differencing throughout the flow field. Unsteady surface pressure predictions as determined by these calculations are depicted in Fig. 7. The results clearly illustrate the need for applying the type-dependent and rotated differencing in unsteady transonic or mixed flows. The central difference calculation provides a spurious surface pressure distribution over an interval on the suction surface which extends somewhat beyond the supersonic region. However, the results of the two calculations are in reasonable agreement on the blade suction surface upstream and downstream of the supersonic region and on the entire blade pressure surface. This suggests that errors caused by inappropriate differencing in supersonic regions and at sonic lines rapidly damp out with increasing distance from the supersonic region.

The second aspect of the unsteady transonic solution to be discussed is the effect of an inaccurate resolution of the steady flow on the linear unsteady calculation. For this purpose two different steady solutions for an inlet Mach number of 0.76 have been used to define the variable coefficients in the unsteady equations. The first is a solution determined on a cascade mesh alone and the second is the steady solution depicted in Fig. 5, which has been determined on both a cascade and a local mesh. The cascade mesh calculation predicts a continuous steady flow with

a surface Mach number distribution which is similar to the continuous distributions shown in Fig. 6, but with a peak Mach number of 1.12 at midchord on the suction surface, and a supersonic region extending from 32% to 68% of blade chord along the suction surface. Calculated unsteady pressures acting on the suction surface, which correspond to the continuous and discontinuous steady solutions, are shown in Fig. 8. Here, transonic differencing is applied and shock phenomena (when present) are captured in the unsteady calculation. Note that the solid curves in Figs. 7 and 8 represent the same unsteady solution. The unsteady predictions based on the accurate discontinuous steady flow are well-behaved with a sharply-defined shock at 64% of blade chord, while those for the continuous steady input reveal violent oscillations in a region centered near x = 0.64. Thus, the first-order perturbation or unsteady solution indicates that a continuous zeroth-order or steady solution is not physically realizable at $M_{-\infty}$ = 0.76, since a small excitation will produce a catastrophic change in the zeroth-order flow.

This feature of the linear perturbation analysis could be a useful one for assessing steady solutions. For example, our steady solution, as determined on both cascade and local meshes for $M_{-\infty}$ = 0.75, indicated a continuous or shock free flow with a peak suction-surface Mach number of 1.06 at midchord. Unsteady predictions for this case were then determined on cascade meshes with axial mesh spacings of 5%, 2.5% and 1.25% of blade chord near midchord. Unsteady predictions on the coarse mesh followed reasonable trends with increasing (from 0.70 to 0.75) inlet Mach number. However, with the finer mesh spacing (2.5% near midchord) the unsteady pressure distribution for $M_{-\infty}$ = 0.75 exhibited large and erratic gradients in a region centered slightly aft of midchord. This behavior was even more pronounced in the results determined on the finest mesh and suggests that the continuous steady flow predicted for an inlet Mach number of 0.75 is not stable or even physically realizable.

The third feature of the unsteady numerical approximation to be discussed is the effect of applying three different approximations at mesh points immediately downstream of the shock. These include: (1) shock capturing; i.e., solving the unsteady differential equation, Eq. (24), using a central difference approximation for the streamwise second derivative of the unsteady potential (c.f. Eq. (54a)); (2) shock fitting assuming that the normal shock displacement (r in Eqs. (29) through (31)), and hence $[\![\phi]\!] = r[\![\Phi_n]\!]$ is prescribed; and (3) shock fitting based on the first-order jump condition for normal shocks, Eq. (32). It should be noted that the unsteady solution based on the simple shock-jump condition, in which r and, hence $[\![\phi]\!]$, is artificially prescribed, satisfies the requirement that no net vorticity be produced at the shock, but mass will not be conserved to first order across the shock. Hence, solutions obtained with this approximation (as well as those obtained by shock capturing) do not represent a uniformly valid first-order approximation to the full, time-dependent, flow field.

For the example, cascade, unsteady, surface pressures resulting from the shock-capturing approximation are represented by the solid curves in Figs. 7 and 8, while those determined by imposing the simple shock-jump condition with $r = [\![\phi]\!] = 0$ and the normal shock-jump condition are represented by the solid and dashed curves, respectively, in Fig. 9. Surface pressure predictions determined by using the simple shock-jump condition are in good agreement with those determined by shock capturing with only slight differences occurring in the immediate vicinity of the shock. However, the surface pressures determined by implementing the formally correct first-order, shock-jump condition are substantially in error in the vicinity of the shock. Such errors can be attributed to difficulties associated with accurately modelling the normal shock-jump condition, particularly on a cascade mesh, and in accurately determining the differences between values of the unsteady potential and unsteady velocity component normal to the shock on the downstream and upstream sides of the shock. The first-order shock-jump condition, Eq. (32), has been derived to provide a perturbation approximation, in which both mass and tangential momentum are conserved to first order, across shocks and, from which, shock displacements can be determined. However, since reasonable numerical solutions have not been determined on a cascade mesh, it appears that a basic prerequisite for assessing both the validity and the usefulness of Eq. (32) would be the implementation of the unsteady numerical approximation on a local mesh consisting of mesh lines normal and parallel to the shock.

Response Predictions for Unstaggered Cascades

Unsteady pressure difference and lift and moment coefficient predictions for unstaggered DCA and flat plate cascades undergoing out-of-phase torsional oscillations (with $\alpha = (1,0)$) about an axis at midchord are shown in Figs. 10 through 15. Unsteady results are presented for low ($\omega = 0.1$), moderate ($\omega = 0.5$) and high ($\omega = 1.0$) frequency motions and for an inlet Mach number range extending from 0.70 to 0.76. The high frequency vibration is the representative one for actual turbomachinery configurations. Steady Mach number distributions for the DCA cascades have been discussed above and are presented in Fig. 5, and the steady flow Mach number is constant throughout the field for the flat plate cascades. Shock capturing has been used in the determination of the unsteady solutions for the discontinuous flows at $M_{-\infty} = 0.76$

The unsteady pressure difference distributions due to the torsional motions of the DCA blades (Figs. 10, 12, and 14) show a substantial variation with inlet Mach number over the midsection (i.e., 30 to 70 percent of chord) of the blade, while a similar variation in inlet Mach number has only a minor impact on the unsteady pressure differences arising from the motions of the flat plate cascades (Figs. 11, 13, and 15). Thus, a comparison of the unsteady pressure difference distributions for the unstaggered DCA and flat plate cascades reveals the dramatic effect of steady Mach number variations, caused by blade thickness and camber, on unsteady response behavior, particularly at transonic Mach numbers. The low-frequency, DCA, pressure-difference distributions (Fig. 10) show very reasonable

trends with increasing inlet Mach number, but the calculated distributions at the
higher frequencies (Figs. 12 and 14) do not inspire a similar degree of confidence.
In particular, the real and imaginary pressure differences for ω = 1.0 indicate a
possibly anomylous behavior in the vicinity of the shock. These distributions
remain relatively flat from the leading edge to approximately 60% of blade chord
and fall or rise extremely rapidly just upstream of the shock. This behavior near
the shock may be attributable to inaccuracies in the vicinity of the shock caused
by performing the unsteady calculations on a cascade mesh. This possibility will
be investigated in detail in our future research.

A detailed comparison of the DCA and flat plate response predictions for out-
of-phase, torsional motions reveals that stability is generally enhanced with
increasing frequency and Mach number. The only exception arises when the increase
in Mach number causes the flow pattern to change from a continuous one to a
discontinuous one. For the continuous flows past the DCA cascade at $M_{-\infty}$ = 0.70,
0.72, and 0.74, the imaginary component of the unsteady pressure difference achieves
relatively large values, which increase with increasing inlet Mach number, upstream
of the point (midchord) at which the steady flow Mach number (Fig. 5) reaches a
maximum on the blade suction and pressure surfaces. This provides a larger clock-
wise moment (Im $\{c_M\}$ < 0) which opposes the blade motion, and hence, stability
enhancement both with increasing Mach number, and relative to the flat plate
cascades operating at the same Mach number. However, large positive unsteady
pressure differences occur just upstream of the shock, but behind the torsional
axis for the discontinuous flows at $M_{-\infty}$ = 0.76. These tend to destabilize the
torsional motions of the DCA blades at $M_{-\infty}$ = 0.76 relative to the situation at lower
inlet Mach numbers and relative to the torsional motions of flat plate blades
operating at the same Mach number.

Results for the unstaggered DCA and flat plate cascades have also been
determined for unit-frequency bending vibrations (Figs. 16 and 17). For clarity,
the real and imaginary pressure difference distributions acting on the reference
DCA blade are plotted separately in Fig. 16. The unsteady pressure difference
distributions due to bending behave in a qualitatively similar manner to the tor-
sional distributions. In particular, substantial differences occur between the DCA
and flat plate pressure difference distributions over the midsection of the blade,
especially at the higher Mach numbers ($M_{-\infty}$ = 0.74 and 0.76), and there is a sig-
nificant reduction in the stability margin for the DCA cascade as the inlet Mach
number is increased from 0.74 to 0.76. For the inlet Mach number range considered,
the predicted stability margin (Im $\{c_L\}$ < 0) for unit-frequency bending vibrations
is greater for the flat plate cascade than for the DCA cascade.

Response Predictions for Staggered Cascades

Unsteady response predictions for staggered (Θ = 45 deg.) DCA and flat plate cascades undergoing out-of-phase torsional vibrations about midchord are shown in Figs. 18 through 21. Results are presented for low (ω = 0.1) and high (ω = 1.0) frequency motions and for inlet Mach numbers of 0.8, 0.85, and 0.9. The steady surface Mach number distributions for the DCA cascade are depicted in Fig. 6, and the unsteady predictions for the discontinuous flows at $M_{-\infty}$ = 0.9 have been determined by shock capturing. A significant difference exists between the flows past the unstaggered (c.f. Fig. 5) and staggered arrays of DCA airfoils. In the former case the steady Mach number has the same value at the inlet and exit, while in the latter, the exit Mach number is substantially lower than the inlet Mach number. This feature can have a substantial impact on the character of the unsteady flow in the far field.

Pressure difference distributions due to the torsional motions of the staggered DCA cascade (Figs. 18 and 20) show a substantial variation with inlet Mach number over the forward-half of the blade. A similar change in inlet Mach number has only a minor impact on the response to low-frequency, flat-plate vibrations (Fig. 19), but a somewhat stronger impact on the high-frequency, flat-plate response (Fig. 21). Unsteady shock phenomena for the staggered DCA cascade operating at $M_{-\infty}$ = 0.9 are not as sharply defined as for the unstaggered DCA cascade operating at $M_{-\infty}$ = 0.76 (Figs. 10 and 14). This is because of the large angles which exist between the axial lines of the (staggered) cascade mesh and the normal shock which impinges on the blade suction surface resulting in some loss in numerical accuracy. Both the low-frequency DCA and flat plate results indicate stability enhancement with increasing Mach number, especially those for the DCA cascade. At low frequency an increase in inlet Mach number leads to an increase in the imaginary component of the unsteady pressure difference over the forward half of the DCA blade (Fig. 18), in particular, just upstream of the shock, and contributes to an increased clockwise moment opposing the blade motion. A similar trend is observed in the low-frequency flat plate results (Fig. 19), but here the increase in Im{Δp} and hence, in the clockwise moment, are relatively small.

The high frequency DCA motions (Fig. 20) at $M_{-\infty}$ = 0.8, 0.85, and 0.9 are superresonant (i.e., acoustic energy persists in the far field). However, acoustic waves only propagate into the far-upstream field since the waves traveling downstream at the lower exit Mach number damp out with distance from the blade row. The high-frequency, flat-plate motions (Fig. 21) are subresonant (i.e., acoustic energy attenuates in the far field) for $M_{-\infty}$ = 0.8, and superresonant for $M_{-\infty}$ = 0.85 and 0.9. For the flat plate cascade, acoustic waves either propagate or attenuate both far upstream and downstream of the blade row since the steady Mach number is constant throughout the flow field. Thus, the unsteady flows at ω = 1.0 past the staggered DCA and flat plate cascades have a very different overall character; however, this is not readily apparent from the surface information depicted in

Figs. 20 and 21. The imaginary component of the unsteady pressure difference due to the high-frequency torsional vibrations of the DCA cascade decreases substantiall: over the forward 30% of the blade producing a decrease in stability margin as the inlet Mach number increases from 0.8 to 0.85. Indeed, the response predictions in Fig. 20 indicate that the DCA torsional vibration at $M_{-\infty}$ = 0.85 is unstable. There is an increase (relative to the $M_{-\infty}$ = 0.85 case) in the imaginary pressure difference over the forward 20% of the DCA blade at $M_{-\infty}$ = 0.9 which contributes to a stable motion at this higher Mach number. Similar trends are observed in the high-frequency, flat-plate results (Fig. 21), but here the torsional motions are stable for the three Mach numbers considered.

CONCLUDING REMARKS

The aerodynamic analysis described in this report is being developed to predict the flow past a finite-deflection oscillating cascade operating under subsonic inlet and exit conditions. In previous studies unsteady subsonic solutions were determined on a cascade mesh for cascades of sharp-edged blades (i.e., flat plate, thin-circular-arc, and double-circular-arc (DCA) airfoils) with blade mean positions aligned with the steady flow (Refs. 17 and 22), and on a cascade mesh and a local leading-edge mesh for cascades of blunt-nosed blades (i.e., NACA 0012 and NACA 65 series airfoils) at incidence relative to the inlet flow (Refs. 23-25). Response predictions for entirely subsonic flows have indicated that a strong coupling can exist between the nonuniform steady and the linear unsteady flow, particularly at high Mach number and/or low vibration frequency.

Under the current phase of the overall research effort, this aerodynamic analysis has been extended for transonic applications. Revised aerodynamic and numerical models have been formulated, and numerical experiments have been conducted to evaluate the solution procedure for cascades operating in the transonic Mach number regime. In particular, first-order or unsteady shock – jump conditions have been formally derived from the integral conservation laws for mass and tangential (to the shock) momentum and included in the aerodynamic model. In addition, type-dependent and rotated differencing strategies, and options for fitting or capturing shocks have been incorporated into the unsteady numerical model. At present the unsteady transonic numerical approximation has only been implemented on a cascade mesh and therefore the calculations described in this report are restricted to cascades of sharp-edged blades with mean positions aligned with the steady flow direction (c.f. Eq. (70)). Further, since it has not been possible to accurately implement the unsteady shock-jump conditions on the cascade mesh, shock capturing has been used for the calculations of discontinuous transonic flows. Work is currently proceeding to improve the resolution of shock phenomena in the linear unsteady calculation by implementing the numerical approximation on a local orthogonal mesh which contains and extends well beyond the supersonic region(s) adjacent to the reference blade surface.

Sample response predictions have been presented for subsonic and transonic flows past vibrating cascades of DCA and flat plate airfoils. Numerical results for a discontinuous transonic flow past an unstaggered DCA cascade illustrate the following: the importance of applying type-dependent and rotated differencing in the unsteady transonic calculation; the effect of an inaccurate resolution of the steady flow on unsteady predictions; and the effect of different approximations at the shock on unsteady transonic solutions. These experiments reveal that errors due to an inaccurate resolution of steady and unsteady shock phenomena rapidly damp out with increasing distance from the shock, and that the first-order solution can be useful for determining the physical realizability of a steady or zeroth-order solution. Brief parametric studies for high subsonic and transonic flows past unstaggered and staggered cascades indicate a dramatic variation in the aerodynamic response to single-degree-of-freedom DCA blade motions with increasing inlet Mach number, while

a similar variation in inlet Mach number has a relatively minor impact on flat plate (i.e., classical linear theory) response predictions. Low-frequency ($\omega = 0.1$) DCA pressure-difference predictions show reasonable trends with increasing inlet Mach number; however, those for moderate ($\omega = 0.5$) and high ($\omega = 1.0$) vibration frequencies show perhaps an anomylous behavior with very steep gradients just upstream and downstream of the shock. Unsteady pressure difference predictions for the discontinuous flows show a sharply defined shock for the unstaggered DCA cascade, but the shock is smeared for blades staggered at 45 deg. This can be attributed to inaccuracies caused by the large number of axial mesh lines which cross the shock in the staggered case.

The examples studied here indicate that improvements in the unsteady solution procedure will be required for an accurate resolution of unsteady shock phenomena, particularly for staggered cascades and high frequency blade motions. The cascade mesh (Fig. 3) is not well suited for resolving the flow near shocks since the axial mesh lines are not "parallel" to the shock. A prerequisite for improving the unsteady solution capability and for assessing both the validity and usefulness of th first-order shock-jump conditions is the implementation of the unsteady numerical approximation on a dense local grid (Fig. 4), which consists of mesh lines normal and parallel to the shock.

Once the foregoing numerical difficulties are resolved, the present analysis will provide an accurate first-order approximation to a weak solution (i.e., a solution admitting discontinuities) of the time-dependent, full-potential equation for small-amplitude blade motions. This analysis formally applies at the reduced frequencies of interest (i.e., $\omega \sim O(1)$) for turbomachinery applications and includes the effects of real blade geometry, mean pressure rise or fall across the blade row, operation at transonic Mach numbers and shocks and their motions in a non-iterative, linear, frequency-domain calculation. It therefore represents a significant advance over the classical linear analyses currently employed in turbomachinery aeroelastic investigations, and over the small-disturbance, unsteady, transonic analyses that have been developed for isolated airfoil applications.

APPENDIX

LIMITING FORMS OF THE GOVERNING EQUATIONS

In this Appendix limiting forms of the aerodynamic equations presented in this report are determined for thin airfoils undergoing small-amplitude unsteady motions normal to the free-stream direction. Our purpose here is to demonstrate that the present aerodynamic model reduces to the often-studied, small-disturbance approximations of potential flow theory (Refs. 1 and 37-39). The latter are derived by assuming that the airfoil produces only small steady and/or unsteady fluctuations in the free-stream flow.

Consider two-dimensional flow in the x,y-plane, with free-stream velocity in the direction of the positive x-axis, past a thin airfoil undergoing small-amplitude harmonic motions. The mean position of the airfoil is located mainly along the x-axis and the unsteady displacement is normal to this axis. Thus, referring to Fig. 22, we let the location of the upper and lower airfoil surfaces be defined by

$$\mathcal{B}(x,y,t) = y_{\pm}(x,t) - \bar{\delta}\bar{f}_{\pm}(x) - \delta f_{\pm}(x)e^{i\omega t} = 0, \qquad x \in \left[0, 1\right] \qquad \text{(A1)}$$

where $\bar{\delta} \ll 1$ and $\delta \ll \bar{\delta}$ are characteristic lengths measuring the projection of the mean airfoil surface on the y-axis and the unsteady amplitude, respectively. The shape functions $\bar{f}_{\pm}(x)$ and $f_{\pm}(x)$ are smooth with x-derivations of order unity everywhere along the chord, and the subscripts + and - refer to the upper and lower surfaces of the airfoil, respectively. With $\bar{\delta} \ll 1$ and $\delta \ll \bar{\delta}$ it is reasonable to expect that the flow (except in small regions near the leading and trailing edges of the airfoil) can be described by a velocity potential of the form

$$\hat{\Phi}(x,y,t) = x + \bar{\phi}(x,y) + \phi(x,y)e^{i\omega t}$$

$$\text{(A2)}$$

$$= x + \bar{\epsilon}\bar{\phi}_1(x,\tilde{y}) + \epsilon\phi_1(x,\tilde{y})e^{i\omega t}$$

where $\bar{\epsilon} \ll 1$ and $\epsilon \ll \bar{\epsilon}$ are functions of $\bar{\delta}$ and δ, respectively such that as $\bar{\epsilon} \to 0$ as $\bar{\delta} \to 0$ and $\epsilon \to 0$ as $\delta \to 0$. In addition, the coordinate scaling $\tilde{y} = \lambda y$ has been introduced and it is assumed that $\bar{\phi}_1$ and ϕ_1 and their derivatives with respect to x and $\tilde{y}$ are of order unity. The parameters λ, $\bar{\epsilon}$ and ϵ are to be determined by the surface boundary condition and the governing differential equation.

Equations governing the steady $\Phi = x + \bar{\phi} = x + \bar{\epsilon}\bar{\phi}_1$, and small-disturbance unsteady, $\phi = \epsilon\phi_1$, potentials (c.f. Eqs. (15), (16), and (17) and Eqs. (22), (24), and (26), respectively) have already been presented for an arbitrary airfoil; i.e., $\bar{\delta} \sim \mathcal{O}(1)$. We now seek consistent approximations to these equations for thin, slightly-cambered airfoils at small mean angles-of-attack relative to the free stream (i.e., $\bar{\delta} \ll 1$).

Steady Flow

After substituting equation (A2) into the steady flow tangency condition, Eq. (17), noting that $\vec{n}_{B,\pm} \approx \pm\, \bar{\delta}\, \bar{f}'_{\pm}\, \vec{e}_x \pm \vec{e}_y$, where $\vec{e}_x$ and $\vec{e}_y$ are unit vectors in the x and y-directions, and neglecting terms of higher order in $\bar{\delta}$, it follows that

$$\bar{\phi}_{1\tilde{y}} = \frac{\bar{\delta}}{\lambda\bar{\epsilon}}\, \bar{f}'_{\pm}, \qquad \text{on } y=0^{\pm},\ x\epsilon\left[0,1\right] \tag{A3}$$

Thus for the expansion, Eq. (A2), to be meaningful

$$\lambda = \mathcal{O}(\bar{\delta}/\bar{\epsilon}) \tag{A4}$$

Upon substituting Eqs. (A2) and (A4) into the steady full-potential equation, Eq. (15), and neglecting terms that are definitely small as ($\bar{\delta} \to 0$) compared to those retained, the following approximate equation is determined for the steady disturbance potential $\bar{\phi}_1$ (x,y)

$$(\bar{\epsilon}/\bar{\delta})^2 \left[1 - M_\infty^2 - \bar{\epsilon}(\gamma+1)M_\infty^2\bar{\phi}_{1x}\right]\bar{\phi}_{1xx} + \bar{\phi}_{1\tilde{y}\tilde{y}} = 0 \tag{A5}$$

Nondegenerate forms of this equation can be determined if $(\bar{\epsilon}/\bar{\delta})^2$ and $|1-M_\infty^2|$ are both of order one; or if, $\bar{\epsilon}^3/\bar{\delta}^2$ is of order one and $|1-M_\infty^2|$ is of order $\bar{\epsilon}$. After returning to the original variables $\bar{\phi}$ and y, the resulting equations are

$$(1 - M_\infty^2)\bar{\phi}_{xx} + \bar{\phi}_{yy} = 0 \quad , \qquad |1-M_\infty^2| \sim \mathcal{O}(1) \tag{A6}$$

and

$$\left[1 - M_\infty^2 - (\gamma+1)M_\infty^2\,\bar{\phi}_x\right]\bar{\phi}_{xx} + \bar{\phi}_{yy} = 0, \qquad |1-M_\infty^2| << 1 \tag{A7}$$

Thus for steady flow past a thin airfoil closely aligned with the free-stream direction the full-potential equation can be approximated by one of the two forms, Eq. (A6) or (A7), depending on the magnitude of the free-stream Mach number. Equation (A6) is the classical linear equation governing small-disturbance subsonic or supersonic flow and equation (A7) is the classical nonlinear equation governing small-disturbance transonic flow. In either approximation the flow tangency condition has the form

$$\bar{\phi}_y = \bar{\delta}\bar{f}'_{\pm}(x) \qquad \text{on} \qquad y=0^{\pm},\ x\epsilon\left[0,1\right] \tag{A8}$$

38

and it follows from Bernoulli's equation, Eq. (16), that the steady-disturbance pressure is given by

$$\bar{p}(x,y) = \hat{P} - P_{\infty} = -2\bar{\phi}_x \tag{A9}$$

Unsteady Flow

After substituting $\Phi(x,y) = \bar{\epsilon}\bar{\phi}_1(x,\tilde{y})$, $\phi(x,y)$, $= \epsilon\phi_1(x,\tilde{y})$, $\vec{r} = \delta f_+(x)\vec{e}_y$, and $\tilde{y} = (\bar{\delta}/\bar{\epsilon})y$ into the unsteady flow tangency equation, Eq. (26), and into the unsteady differential equation, Eq. (24), and neglecting terms that vanish in the limit $\delta << \bar{\delta} \to 0$, it follows that

$$\phi_{1\tilde{y}} = \frac{\bar{\epsilon}}{\bar{\delta}}\frac{\delta}{\epsilon}\left[f'_{\pm}(x) + i\omega f_{\pm}(x)\right], \qquad \text{on} \quad y = 0^{\pm}, \; x\epsilon\left[0,1\right] \tag{A10}$$

and

$$(\bar{\epsilon}/\bar{\delta})^2\left[1 - M_{\infty} - \bar{\epsilon}(\gamma+1)M_{\infty}^2\bar{\phi}_{1x}\right]\phi_{1xx} + \phi_{1\tilde{y}\tilde{y}} - 2i\omega M_{\infty}^2\phi_{1x}$$

$$-(\bar{\epsilon}^3/\bar{\delta}^2)M_{\infty}^2\left[2i\omega\bar{\phi}_{1x} + (\gamma+1)\bar{\phi}_{1xx}\right]\phi_{1x} + \omega^2 M_{\infty}^2\phi_1 \tag{A11}$$

$$-(\bar{\epsilon}^3/\bar{\delta}^2)\,i\omega M_{-\infty}^2(\gamma-1)\bar{\phi}_{1xx}\phi_1 = 0$$

Thus for both sides of Eq. (A10) to be of the same order

$$\delta/\epsilon = \mathcal{O}(\bar{\delta}/\bar{\epsilon}) \tag{A12}$$

If the ratio $(\bar{\epsilon}/\bar{\delta})$ and the frequency ω are both of order unity, equation (A11) reduces to the classical linear equation of unsteady subsonic or supersonic flow theory (Refs. 37, 38); i.e.,

$$(1 - M_{\infty}^2)\phi_{xx} + \phi_{yy} - 2i\omega M_{\infty}^2\phi_x + \omega^2 M_{\infty}^2\phi = 0 \tag{A13}$$

If, in addition, $|1-M_{\infty}^2|$ is of order $\bar{\epsilon}$, the first term in Eq. (A13) can be eliminated to recover the linear equation of unsteady transonic flow theory (Ref. 39). The corresponding flow tangency and unsteady pressure relations are

$$\phi_y = f'_{\pm} + i\omega f_{\pm}, \qquad \text{on} \; y = 0^{\pm}, \; x\epsilon\left[0,1\right] \tag{A14}$$

and

$$p = -2(\phi_x + i\omega\phi) \tag{A15}$$

where $\hat{P} \approx P_\infty + \bar{p} + pe^{i\omega t}$. In this approximation there is no coupling between the small-disturbance steady and unsteady flows, and equations (A13)-(A15) could be derived under the less restrictive assumption that $\delta \ll 1$ rather than $\delta \ll \bar{\delta} \ll 1$.

If $(\bar{\epsilon}^3/\bar{\delta}^2)$ is of order unity and $|1-M_\infty|$ and ω are both of order $\bar{\epsilon}$, Eq. (A11) reduces to the linear, low-frequency, unsteady transonic equation (Refs. 3-6); i.e.,

$$\left[1 - M_\infty^2 - (\gamma+1)M_\infty^2 \bar{\phi}_x\right]\phi_{xx} + \phi_{yy} - 2i\omega M_\infty^2 \phi_x$$

$$- (\gamma+1)M_\infty^2 \bar{\phi}_{xx}\phi_x = i\omega M_\infty^2 \left[2\bar{\phi}_x\phi_x - (\gamma-1)\bar{\phi}_{xx}\phi\right] - \omega^2 M_\infty^2 \phi \tag{A16}$$

The corresponding flow tangency and unsteady pressure relations are

$$\phi_y - \delta f' = i\omega\delta f \tag{A17}$$

and

$$p + 2\phi_x = -2i\omega\phi \tag{A18}$$

The right-hand-sides of equations (A16) through (A18) are of order $\bar{\epsilon}$ and hence, should be eliminated for a strict observance of the order of magnitude analysis. However, these terms are often retained in an effort to extend the range of applicability of the low-frequency transonic approximation and to provide a bridge to the linear unsteady transonic theory. In the low-frequency, transonic approximation the dependence of the unsteady flow on the underlying steady flow is reflected by the appearance of the $\bar{\phi}_x$ and $\bar{\phi}_{xx}$ terms in the governing differential equation, Eq. (A16) If steady and unsteady disturbances are assumed to be of the same order of magnitude then a similar order of magnitude analysis of the time-dependent, full-potential equation will yield the nonlinear, low-frequency, unsteady, transonic approximation studied by Ballhaus and Goorjian (Ref. 7).

In the derivation of the linear unsteady equations described earlier in this report, terms have been eliminated simply on the basis that unsteady disturbances are small relative to steady disturbances. The analysis in this Appendix demonstrat

that these general linear equations reduce to familiar limiting forms for small steady ($\bar{\delta} \ll 1$) and unsteady ($\delta \ll \bar{\delta}$) disturbances provided that additional scalings on λ, ω, and $|1-M_\infty^2|$ are considered. This suggests that the general linear aerodynamic model will be applicable to transonic ($|1-M_\infty| \ll 1$) as well as to subsonic or supersonic ($|1-M_\infty| \sim \mathcal{O}(1)$) flows for vibration frequencies of order unity or smaller.

REFERENCES

1. Tijdeman, H. and R. Seebass: Transonic Flow Past Oscillating Airfoils. Annual Review of Fluid Mechanics, Vol. 12, 1980, pp. 181-222.

2. Platzer, M. F.: Unsteady Flow in Turbomachines - A Review of Current Developments. Unsteady Aerodynamics, AGARD CP-227, 1977.

3. Ehlers, F. E.: A Finite Difference Method for the Solution of the Transonic Flow Around Harmonically Oscillating Wings. NASA CR-2257, July 1974.

4. Traci, R. M., E. D. Albano and J. L. Farr: Perturbation Method for Transonic Flows About Harmonically Oscillating Airfoils. AIAA Journal, Vol. 14, No. 9, pp. 1258-1265, September 1976.

5. Weatherill, W. H. and F. E. Ehlers: Analysis of Transonic Flow About Harmonically Oscillating Airfoils and Wings. Paper No. 80-0149, AIAA 18th Aerospace Sciences Meeting, Pasadena, CA, January 1980.

6. Fung, K-Y, N. J. Yu, and R. Seebass: Small Unsteady Perturbations in Transonic Flows. AIAA Journal, Vol. 16, No. 8, pp. 815-822, August 1978.

7. Ballhaus, W. F. and P. M. Goorjian: Implicit Finite-Difference Computations of Unsteady Transonic Flows About Airfoils. AIAA Journal, Vol. 15, No. 12, pp. 1728-1735, December 1977.

8. Ballhaus, W. F. and P. M. Goorjian: Computation of Unsteady Transonic Flows by the Indicial Method. AIAA Journal, Vol. 16, No. 2, pp. 117-124, February 1978.

9. Isogai, K.: Calculation of Unsteady Transonic Flow Over Oscillating Airfoils Using the Full Potential Equation. Paper No. 77-448, AIAA/ASME 18th Structures Structural Dynamics and Materials Conference, San Diego, CA, March 1977.

10. Chipman, R. and A. Jameson: Fully Conservative Numerical Solutions for Unsteady Irrotational Transonic Flow About Airfoils. Paper No. 79-1555, AIAA 12th Fluid and Plasma Dynamics Conference, Williamsburg, VA, July 23-25, 1979.

11. Goorjian, P. M.: Implicit Computations of Unsteady Transonic Flow Governed by the Full Potential Equation in Conservation Form. Paper No. 80-0150, AIAA 18th Aerospace Sciences Meeting, Pasadena, CA, January 14-16, 1980.

12. Tijdeman, H.: On the Motion of Shock Waves on an Airfoil with Oscillating Flap. Symposium Transsonicum II, Springer-Verlag, 1975, pp. 49-56.

13. Houwink, R. and J. van der Vooren: Some Results of an Improved Version of LTRAN2 for Computing Unsteady Airloads on Airfoils Oscillating in Transonic Flow. Ppaer No. 79-1443, AIAA 12th Fluid and Plasma Dynamics Conference, Williamsburg, VA, July 24-26, 1979.

14. Rizzetta, D. P. and W. C. Chin: Effect of Frequency in Unsteady Transonic Flow. AIAA Journal, Vol. 17, No. 7, July 1979, pp. 779-781.

15. Kerlick, G. D. and D. Nixon: A High-Frequency Transonic Small Distrubance Code for Unsteady Flows in a Cascade. Paper No. 82-0955, AIAA/ASME 3rd Joint Thermophysics, Fluids, Plasma and Heat Transfer Conference, St. Louis, MO, June 7-11, 1982.

16. Whitehead, D. S.: Unsteady Aerodynamics in Turbomachinery. Special Course on Unsteady Aerodynamics, AGARD Report No. 679, June 1980.

17. Verdon, J. M. and J. R. Caspar: Subsonic Flow Past an Oscillating Cascade with Finite Mean Flow Deflection. AIAA Journal, Vol. 18, No. 5, May 1980, pp. 540-548.

18. Atassi, H. and T. J. Akai: Effect of Blade Loading and Thickness on the Aerodynamics of Oscillating Cascades. Paper No. 78-227, AIAA 16th Aerospace Sciences Meeting, Huntsville, AL, January 16-18, 1978.

19. Whitehead, D. S. and R. J. Grant: Force and Momentum Coefficients for High Deflection Cascades. Aeroelasticity in Turbomachines, P. Suter (editor), Proceedings of the Second International Symposium held in Lausanne, Switzerland, September 8-12, 1980, Juris-Verlag Zurich, 1981, pp. 85-127.

20. Caruthers, J. E.: Aerodynamic Analysis of Cascaded Airfoils in Unsteady Rotational Flow. Aeroelasticity in Turbomachines, P. Suter (Editor), Proceedings of the Second International Symposium held in Lausanne, Switzerland, September 8-12, 1980, Juris-Verlag Zurich, 1981, pp. 31-64.

21. McNally, W. D. and P. M. Sockol: Computational Methods for Internal Flows with Emphasis on Turbomachinery. NASA Technical Memorandum 82764, November 1981.

22. Caspar, J. R. and J. M. Verdon: Numerical Treatment of Unsteady Subsonic Flow Past an Oscillating Cascade. AIAA Journal, Vol. 19, No. 12, December 1981, pp. 1531-1539.

23. Verdon, J. M. and J. R. Caspar: Development of an Unsteady Aerodynamic Analysis for Finite-Deflection Subsonic Cascades. NASA CR-3455, prepared under contract NAS3-21981 for NASA Lewis Research Center, September 1981.

24. Verdon, J. M. and J. R. Caspar: Development of a Linear Unsteady Aerodynamic Analysis for Finite-Deflection Subsonic Cascades. AIAA Journal, Vol. 20, No. 9 September 1982, pp. 1259-1267.

25. Carta, F. O.: Unsteady Gapwise Periodicity of Oscillating Cascaded Airfoils. Paper No. 82-GT-286, ASME International Gas Turbine Conference and Exhibit, London, England, April 18-22, 1982.

26. Jameson, A.: Iterative Solution of Transonic Flows Over Airfoils and Wings Including Flows at Mach 1. Communication of Pure and Applied Mathematics, Vol. 27, 1974, pp. 283-309.

27. Murman, E. H. and J. D. Cole: Calculation of Plane Steady Transonic Flows. AIAA Journal, Vol. 9, No. 1, pp. 114-121, January 1971.

28. Murman, E. H.: Analysis of Embedded Shock Waves Calculated by Relaxation Methods. AIAA Journal, Vol. 12, No. 5, May 1974, pp. 626-633.

29. Aris, A.: Vectors, Tensors, and the Basic Equations of Fluid Mechanics. Prentice-Hall, Inc., Englewood Cliffs, New Jersey, 1962, p. 122.

30. Whitham, G. B.: Linear and Nonlinear Waves. John Wiley & Sons, New York, 1974, pp. 172-176.

31. Verdon, J. M., J. J. Adamczyk and J. R. Caspar: Subsonic Flow Past an Oscillating Cascade with Steady Blade Loading - Basic Formulation. Unsteady Aerodynamics, R. B. Kinney (ed.), Proceedings of a Symposium held at the University of Arizona, Tucson, AZ, March 1975, Vol. II, pp. 827-851.

32. Carta, F. O.: Coupled Blade-Disk-Shroud Flutter Instabilities in Turbojet Engine Rotors. Transactions of the ASME, Journal of Engineering for Power, Series A, Vol. 89, No. 3, July 1967, pp. 419-427.

33. Van Dine, C. P.: An Algorithm for the Optimization of Trajectories with Associated Parameters. AIAA Journal, Vol. 7, March 1969, pp. 400-405.

34. Fung, Y. C.: An Introduction to the Theory of Aeroelasticity. John Wiley and Sons, Inc., New York, 1955, pp. 166-168.

35. Caspar, J. R., D. E. Hobbs and R. L. Davis: Calculation of Two-Dimensional Potential Cascade Flow Using Finite Area Methods. AIAA Journal, Vol. 18, January 1980, pp. 103-109.

36. Caspar, J. R.: Unconditionally Stable Calculation of Transonic Potential Flow Through Cascades Using an Adaptive Mesh for Shock Capture. Paper No. 82-GT-238 ASME International Gas Turbine Conference and Exhibit, London, England, April 18-22, 1982.

37. Ashley, H. and M. Landahl: <u>Aerodynamics of Wings and Bodies</u>. Addison-Wesley Publishing Company, Inc., Reading, MA, 1965, pp. 81-86, 230-233 and 245-249.

38. Miles, J. W.: <u>The Potential Theory of Unsteady Supersonic Flow</u>. Cambridge University Press, Cambridge, England, 1959, pp. 4-13.

39. Landahl, M.: <u>Unsteady Transonic Flow</u>. Pergamon Press, New York, 1961, pp. 1-21.
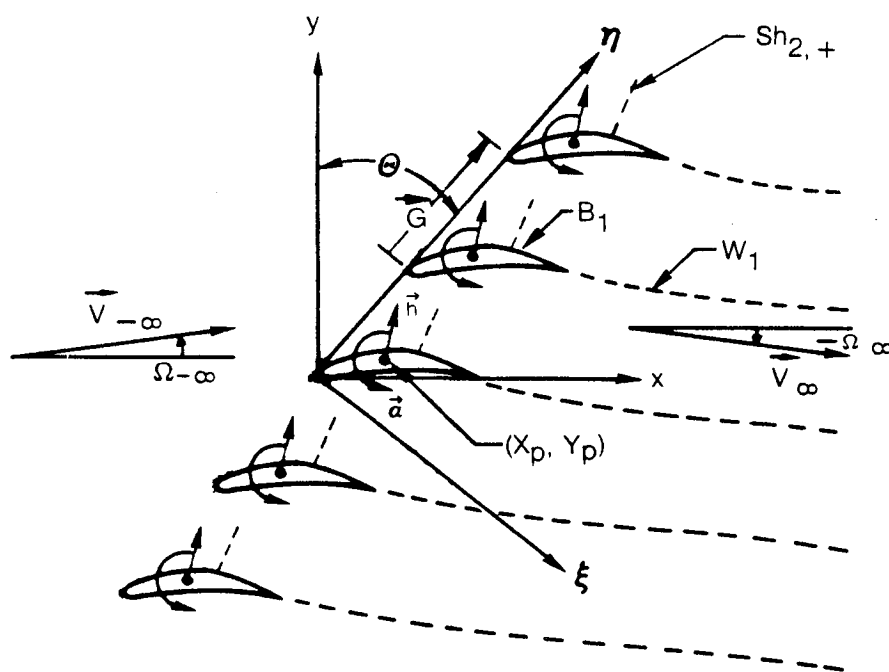
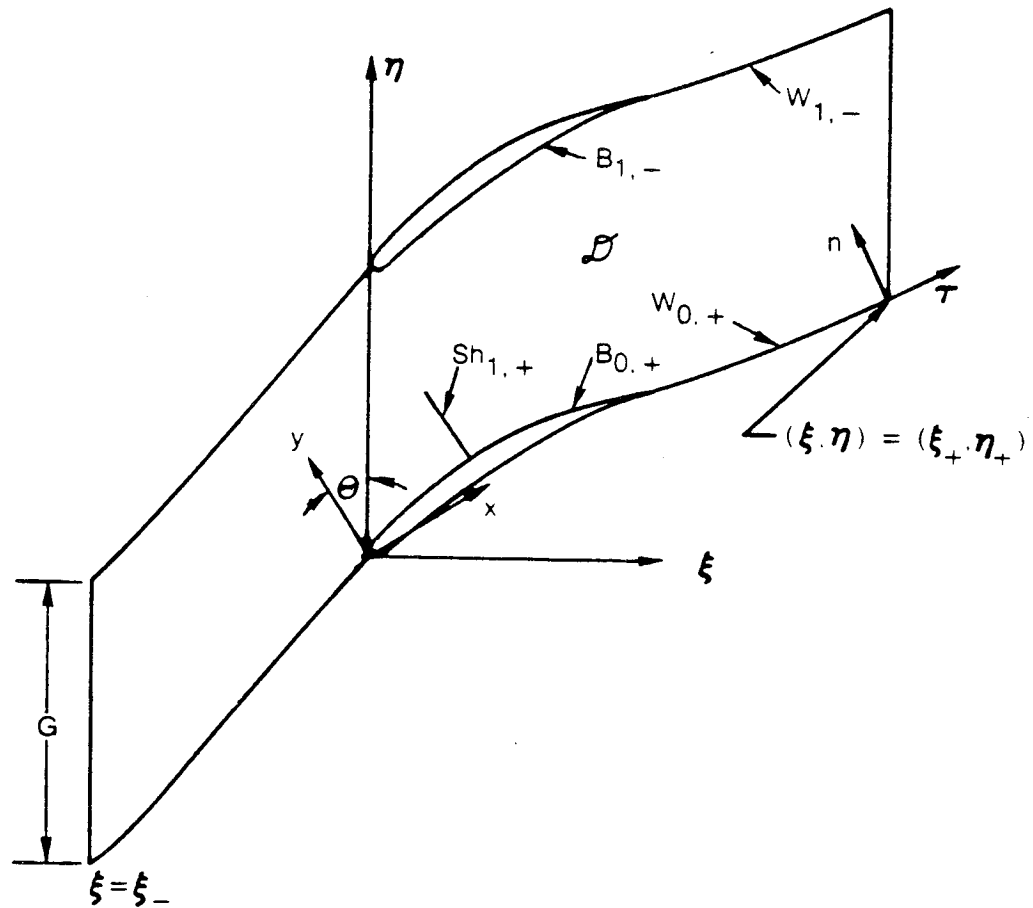**Fig. 1 Two-Dimensional Oscillating Transonic Cascade with Finite Mean-Flow Deflection**

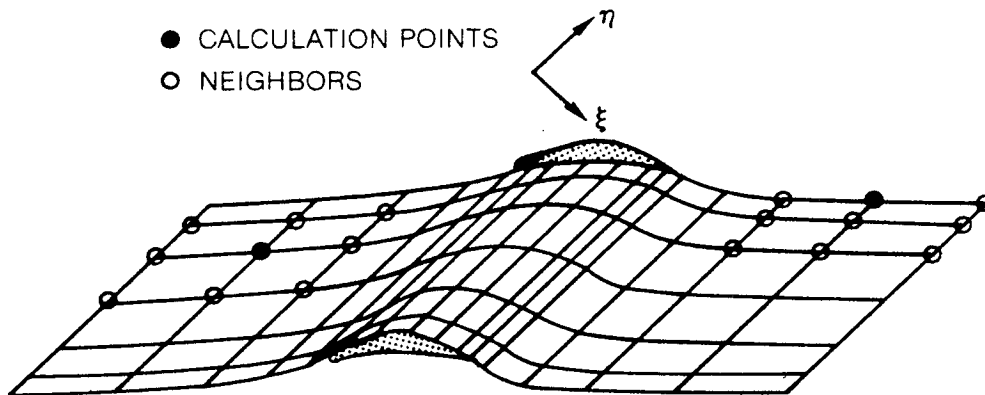**Fig. 2 Extended Blade-Passage Solution Domain**

● CALCULATION POINTS
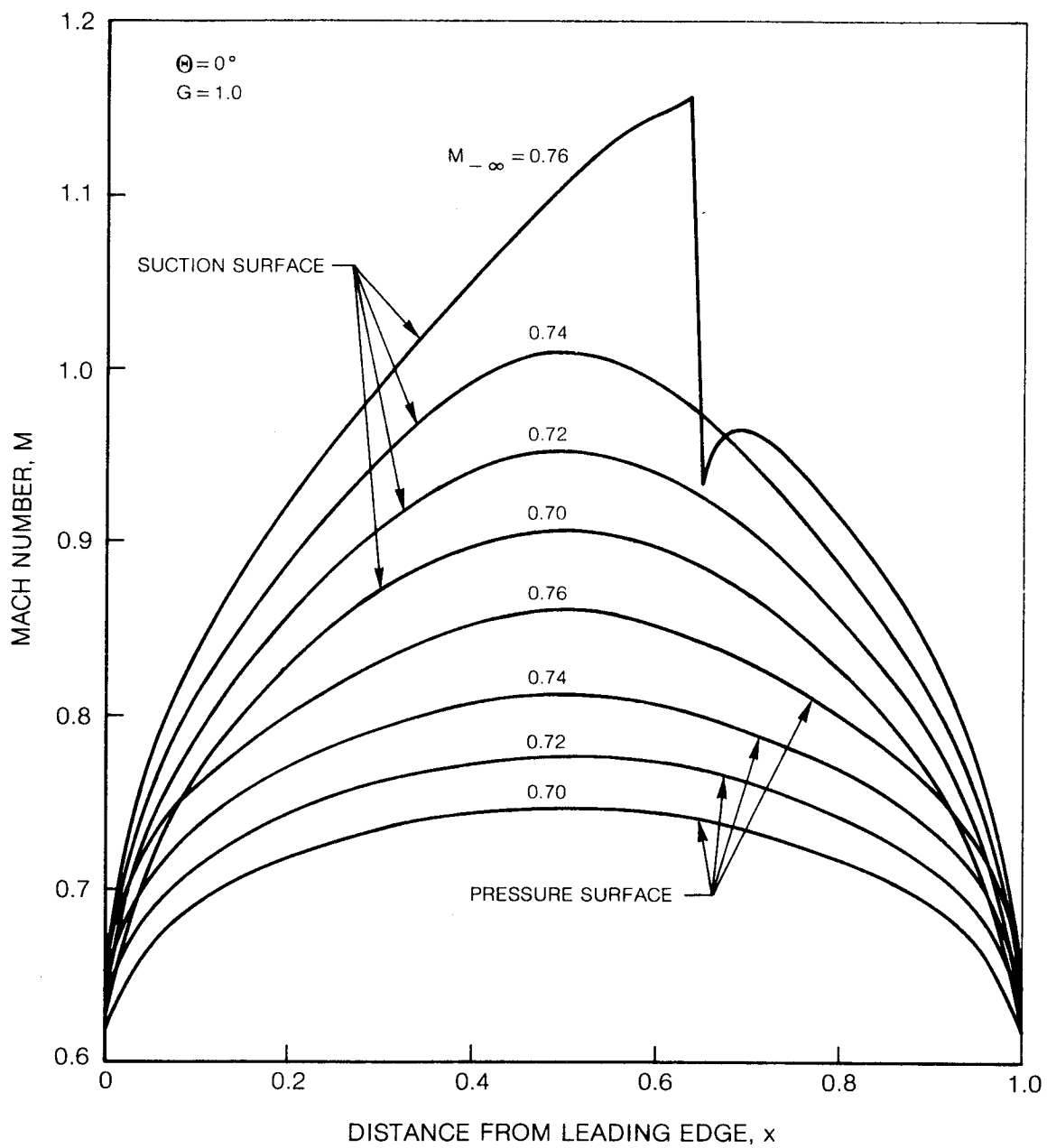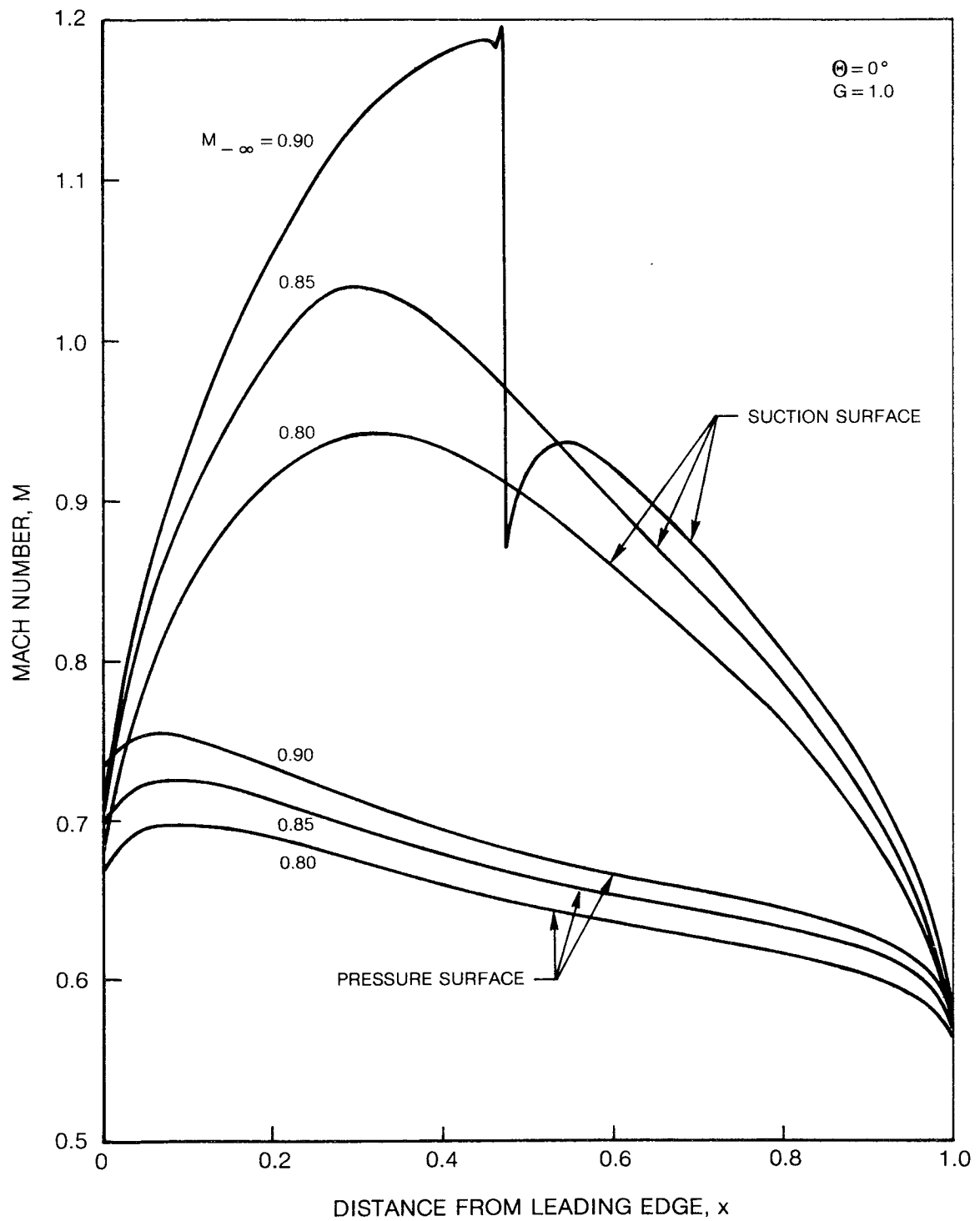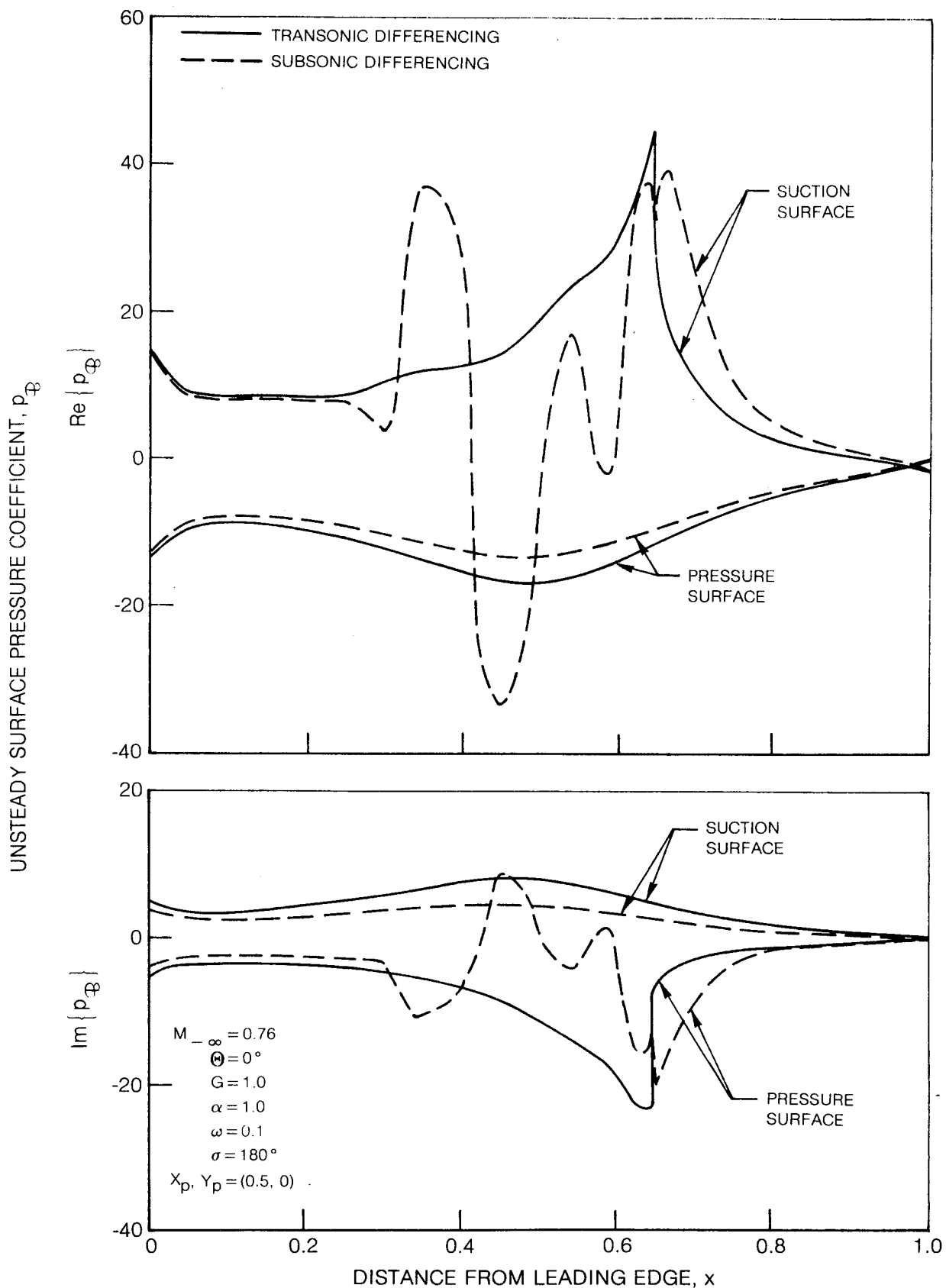○ NEIGHBORS

η
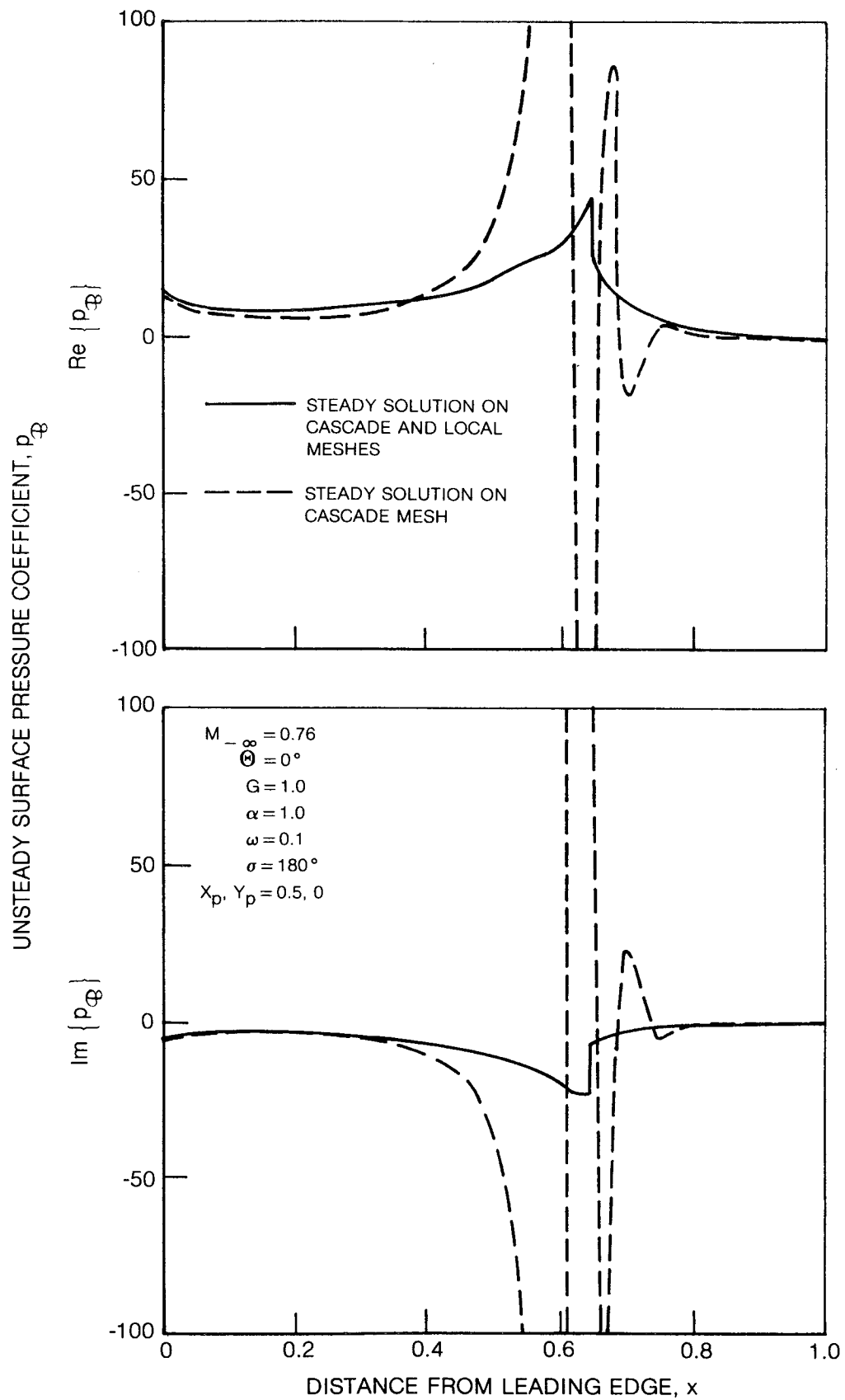
ξ

Fig. 3 Cascade Mesh
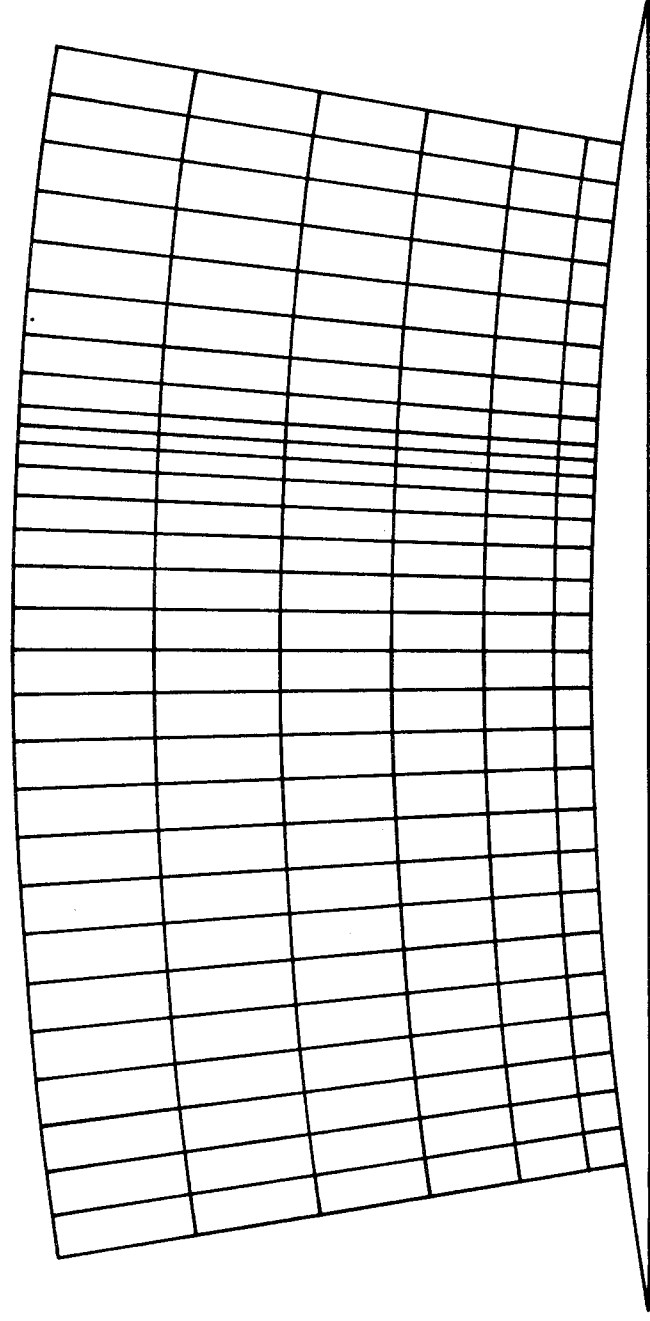
Fig. 4 Local Shock Mesh

Fig. 5 Surface Mach Number Distributions for an Unstaggered DCA Cascade

Fig. 6 Surface Mach Number Distributions for a Staggered DCA Cascade
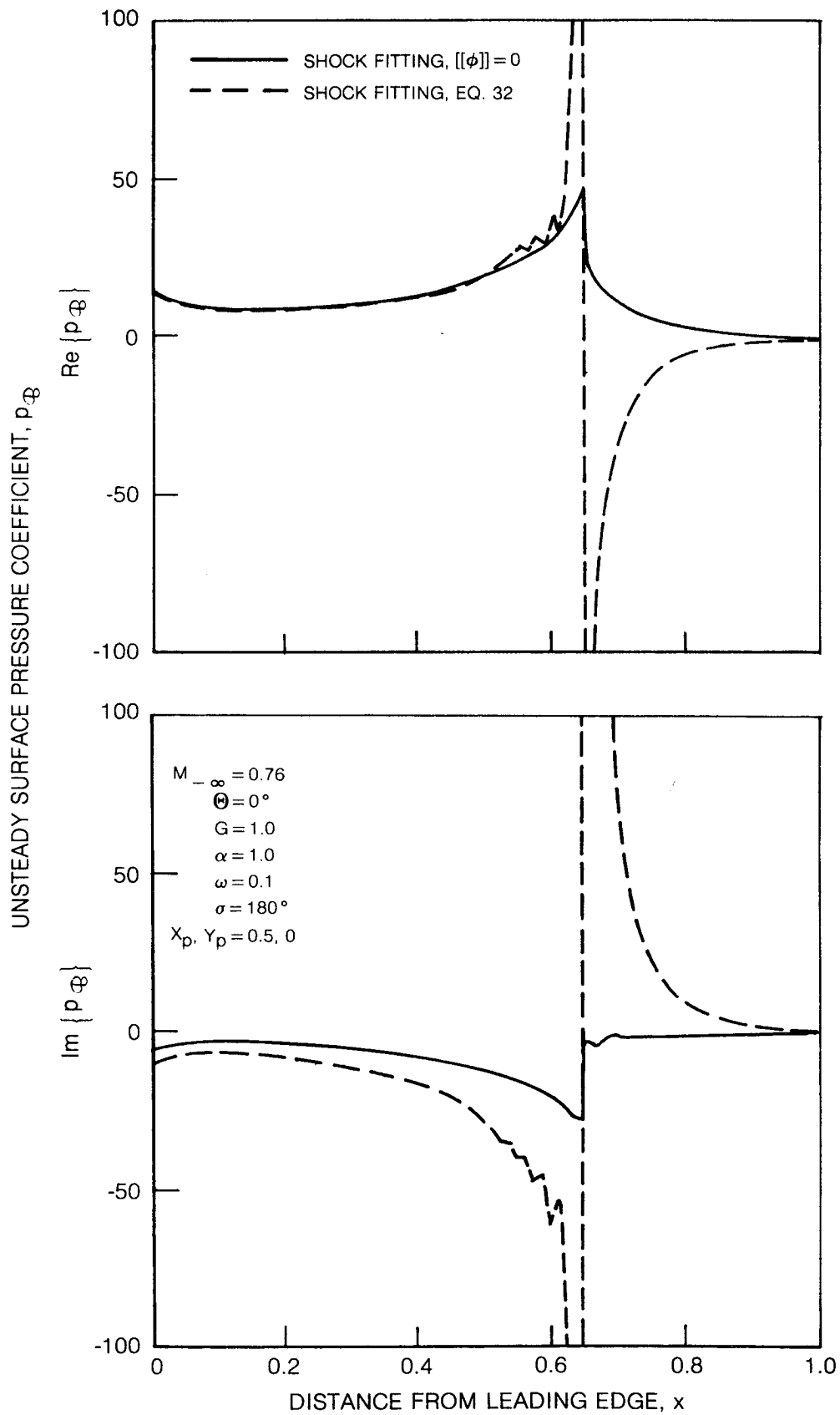
Fig. 7 Effect of Transonic Differencing Strategies on Unsteady Surface-Pressure Predictions
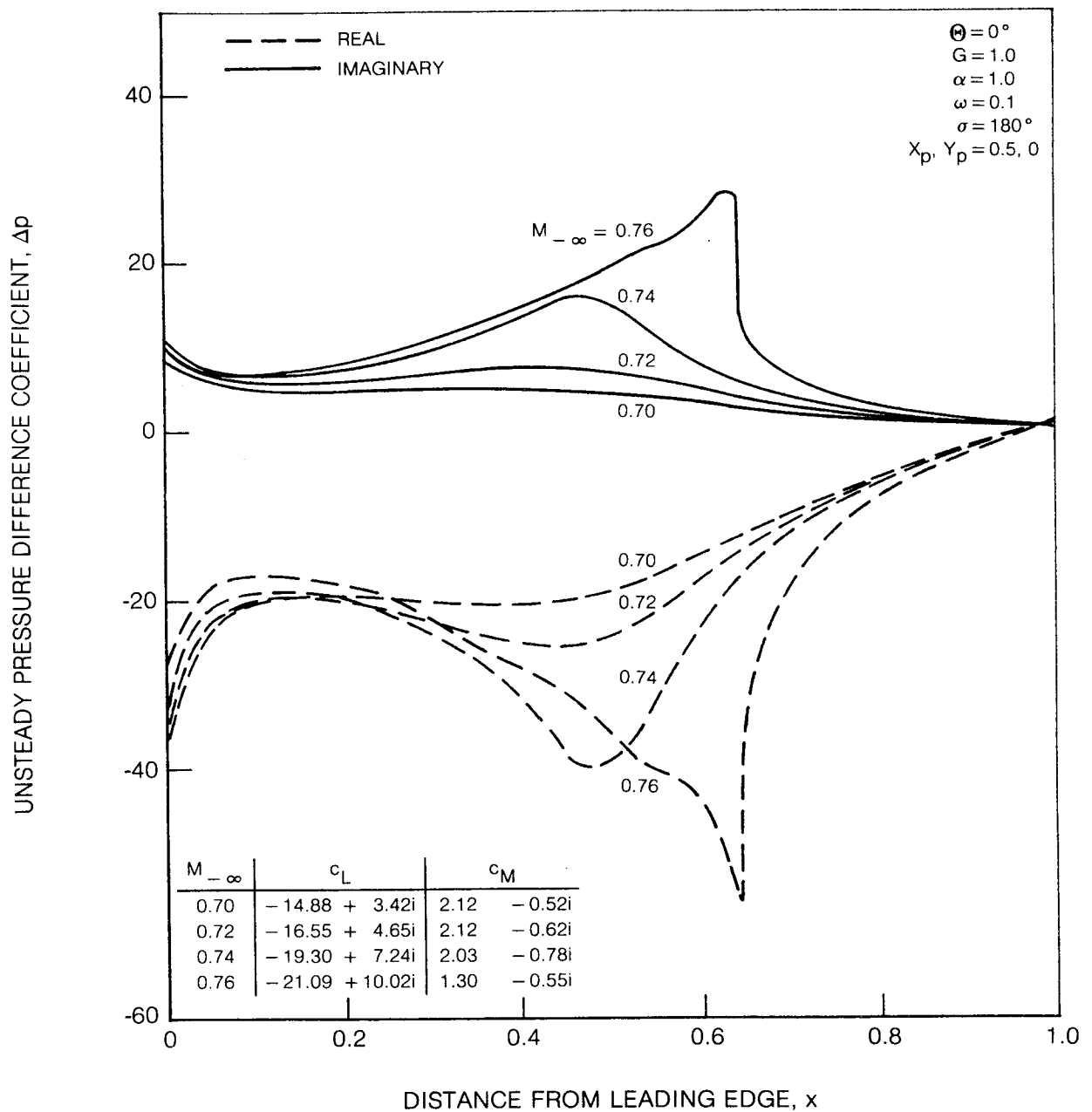
**Fig. 8 Effect of Steady Flow Resolution on Unsteady Suction-Surface Pressure Predictions**

Fig. 9 Effect of Numerical Treatment at Shock on Unsteady Suction-Surface Pressure Predictions

82—9—10—6

UNSTEADY PRESSURE DIFFERENCE COEFFICIENT, Δp

- - - - REAL
——— IMAGINARY

$\Theta = 0°$
$G = 1.0$
$\alpha = 1.0$
$\omega = 0.1$
$\sigma = 180°$
$X_p, Y_p = 0.5, 0$

$M_{-\infty} = 0.76$

0.74

0.72

0.70

0.70
0.72
0.74
0.76

$M_{-\infty}$	c_L		c_M	
0.70	-14.88	$+ \ 3.42i$	2.12	$-0.52i$
0.72	-16.55	$+ \ 4.65i$	2.12	$-0.62i$
0.74	-19.30	$+ \ 7.24i$	2.03	$-0.78i$
0.76	-21.09	$+10.02i$	1.30	$-0.55i$

DISTANCE FROM LEADING EDGE, x

Fig. 10 Effect of Inlet Mach Number on Unsteady Response due to Low-Frequency Torsional Vibrations of an Unstaggered DCA Cascade
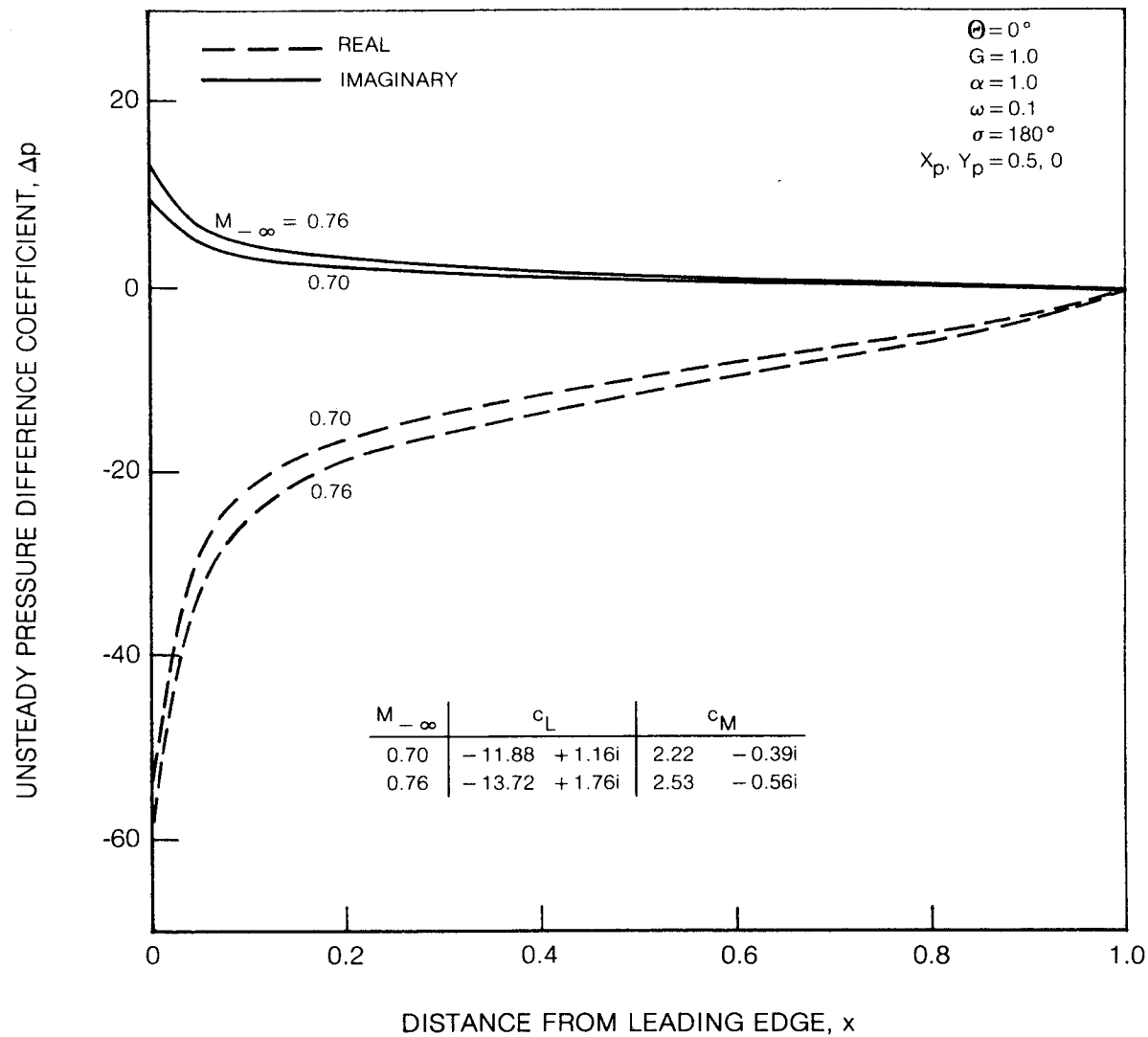
Fig. 11 Effect of Inlet Mach Number on Unsteady Response due to Low-Frequency Torsional Vibrations of a Flat Plate Cascade
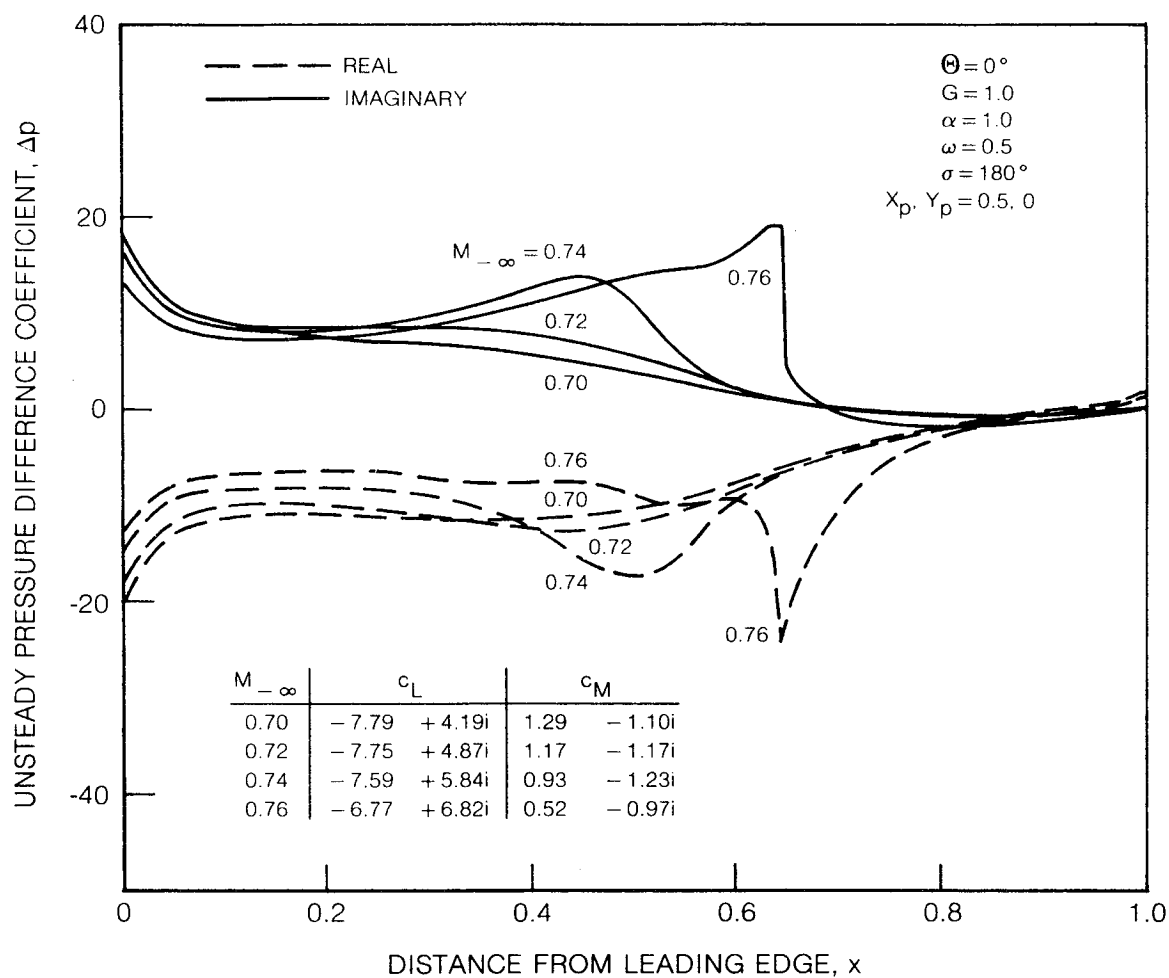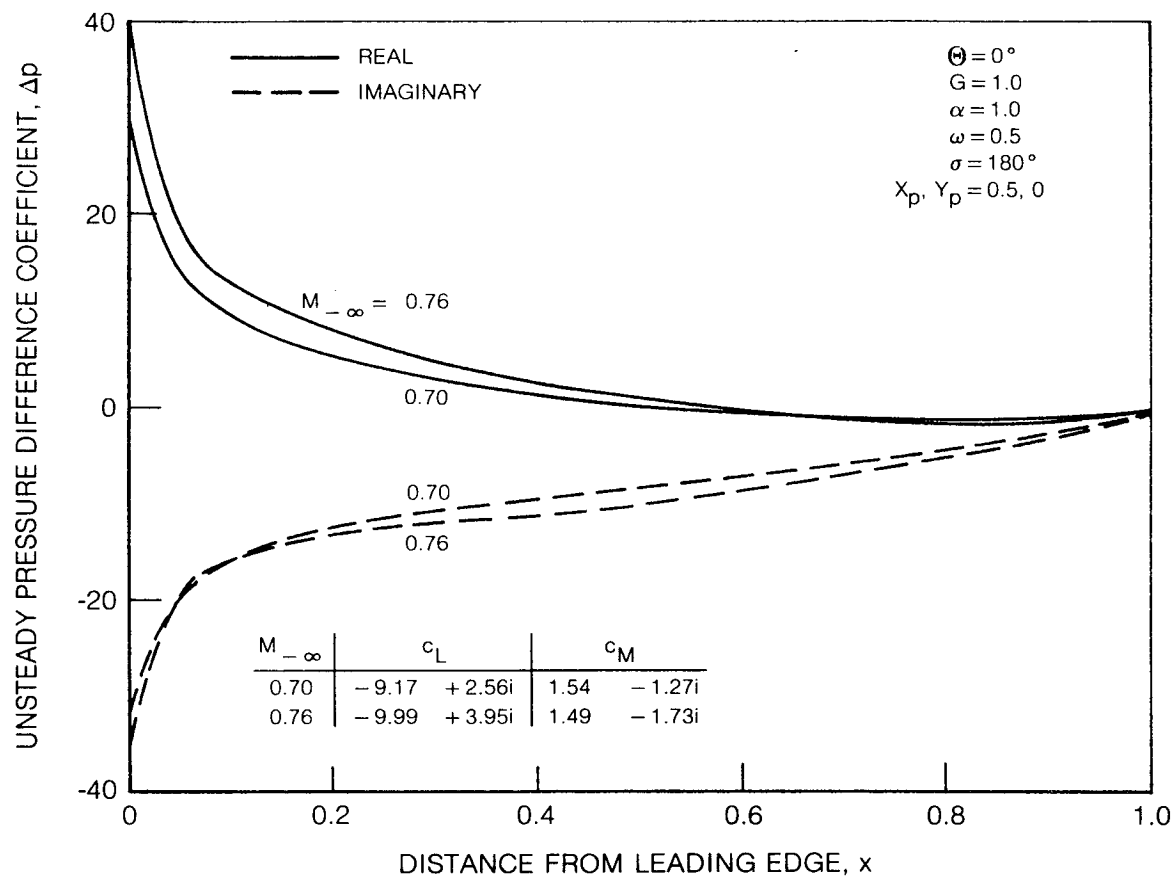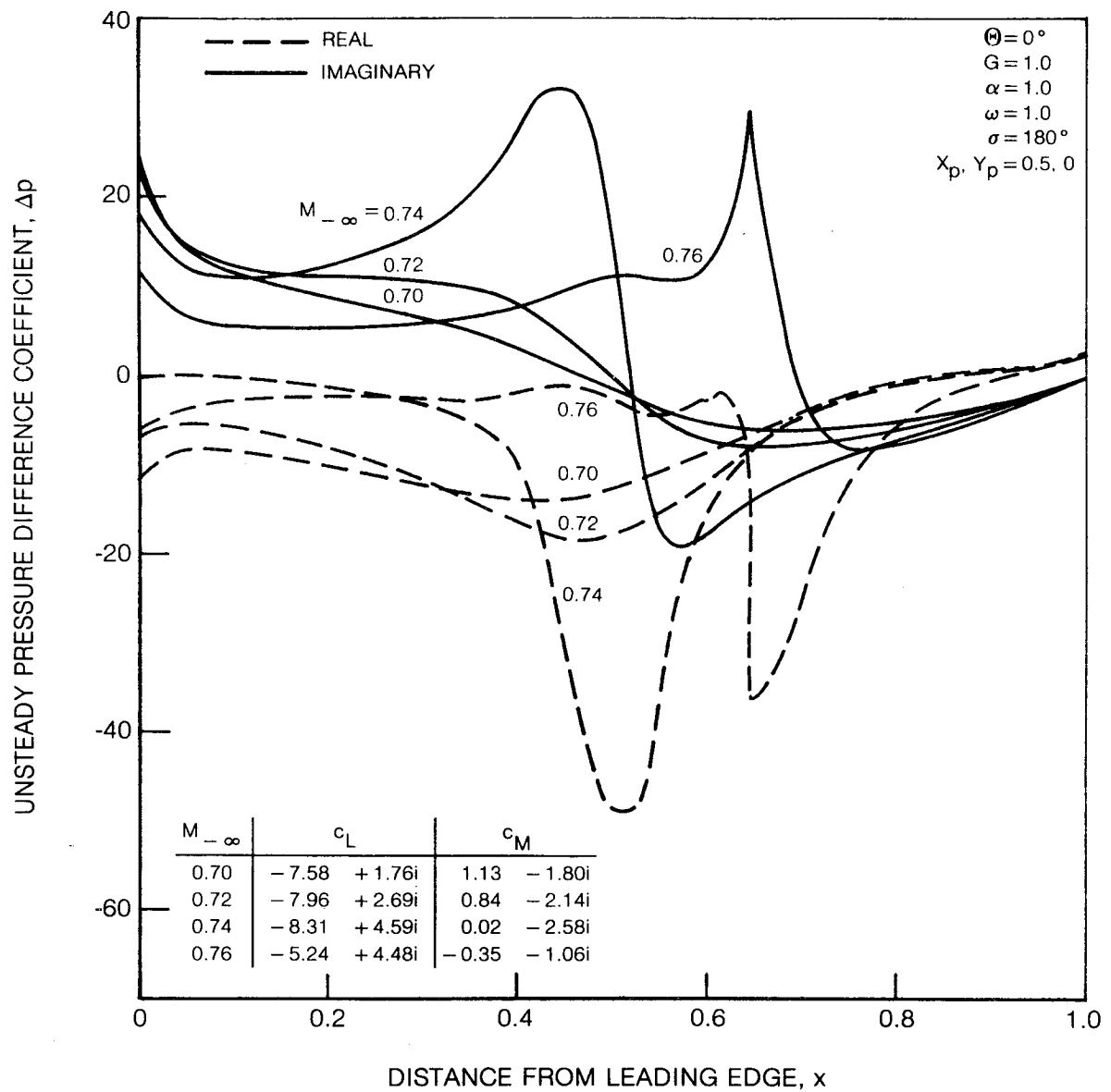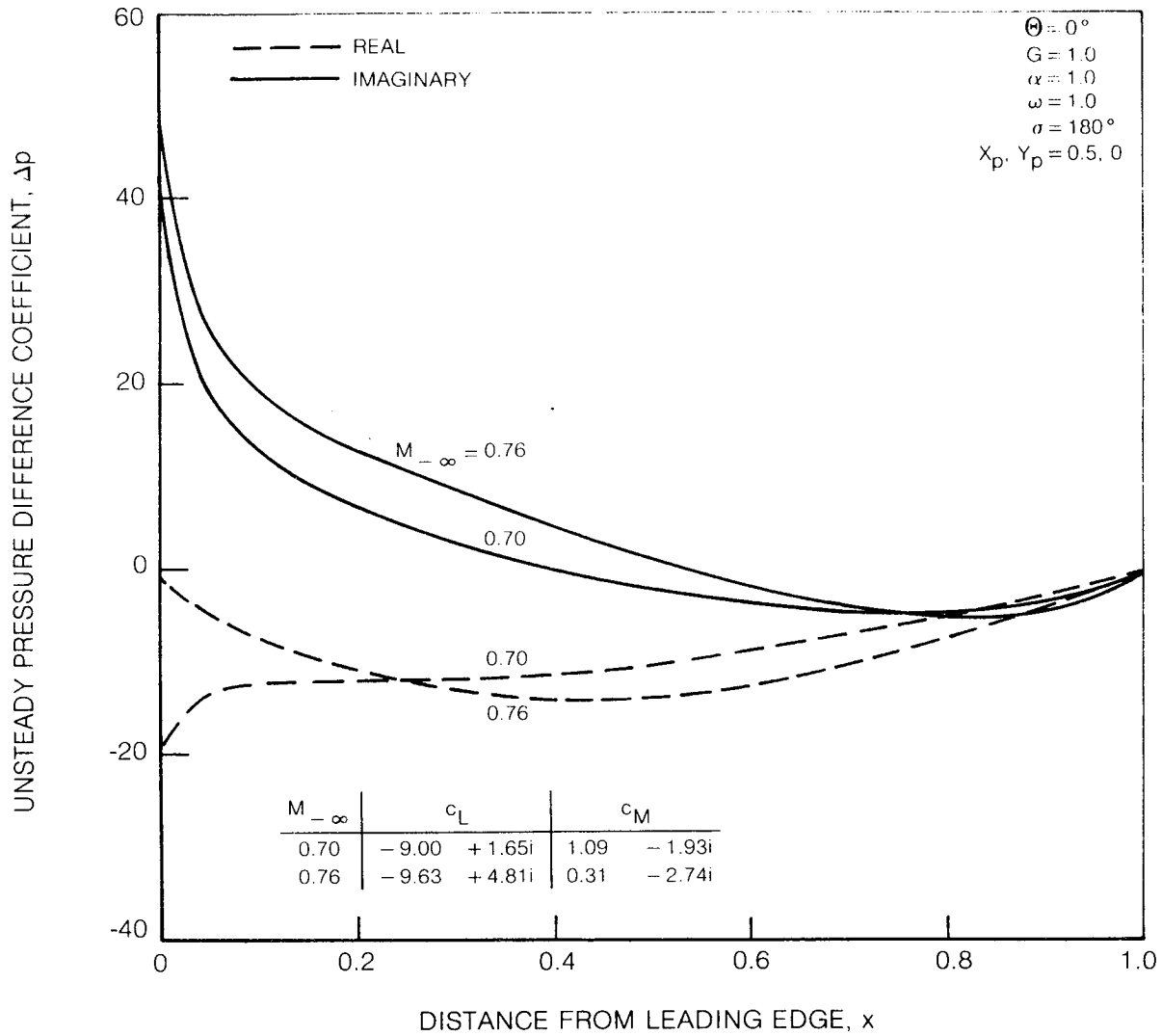
Fig. 12 Effect of Inlet Mach Number on Unsteady Response due to Moderate-Frequency Torsional Vibrations of an Unstaggered DCA Cascade

Fig. 13 Effect of Inlet Mach Number on Unsteady Response due to Moderate-Frequency Torsional Vibrations of a Flat Plate Cascade

The chart shows Unsteady Pressure Difference Coefficient, Δp versus Distance from Leading Edge, x. Conditions: $\Theta = 0°$, $G = 1.0$, $\alpha = 1.0$, $\omega = 1.0$, $\sigma = 180°$, $X_p, Y_p = 0.5, 0$. Legend: REAL (dashed), IMAGINARY (solid). Curves labeled for $M_{-\infty} = 0.70, 0.72, 0.74, 0.76$.

$M_{-\infty}$	c_L		c_M	
0.70	-7.58	$+1.76i$	1.13	$-1.80i$
0.72	-7.96	$+2.69i$	0.84	$-2.14i$
0.74	-8.31	$+4.59i$	0.02	$-2.58i$
0.76	-5.24	$+4.48i$	-0.35	$-1.06i$

Fig. 14 Effect of Inlet Mach Number on Unsteady Response due to High-Frequency Torsional Vibrations of an Unstaggered DCA Cascade
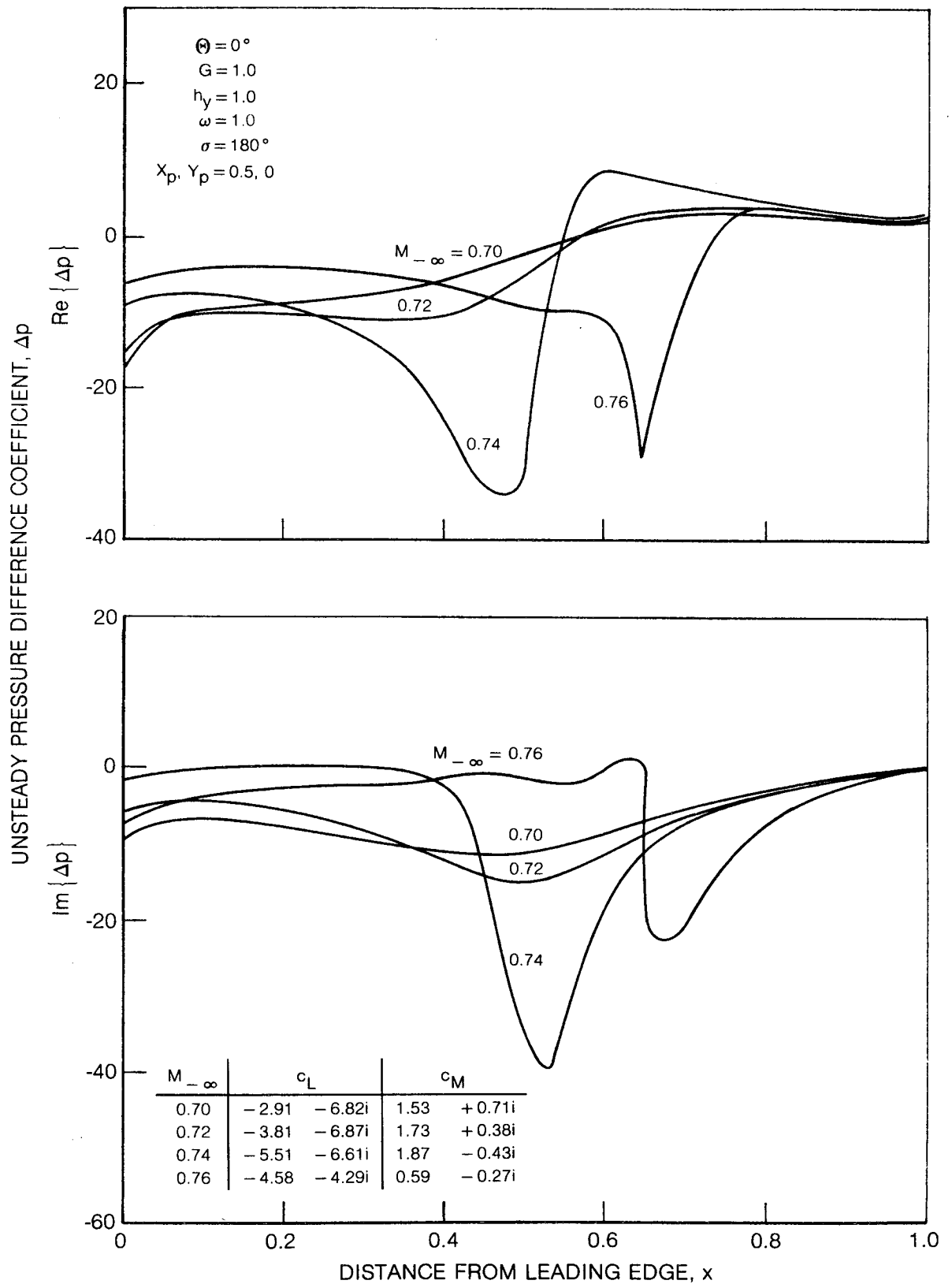
UNSTEADY PRESSURE DIFFERENCE COEFFICIENT, Δp

- - - - REAL
——— IMAGINARY

$\Theta = 0°$
$G = 1.0$
$\alpha = 1.0$
$\omega = 1.0$
$\sigma = 180°$
$X_p, Y_p = 0.5, 0$

$M_{-\infty} = 0.76$

0.70

0.70

0.76

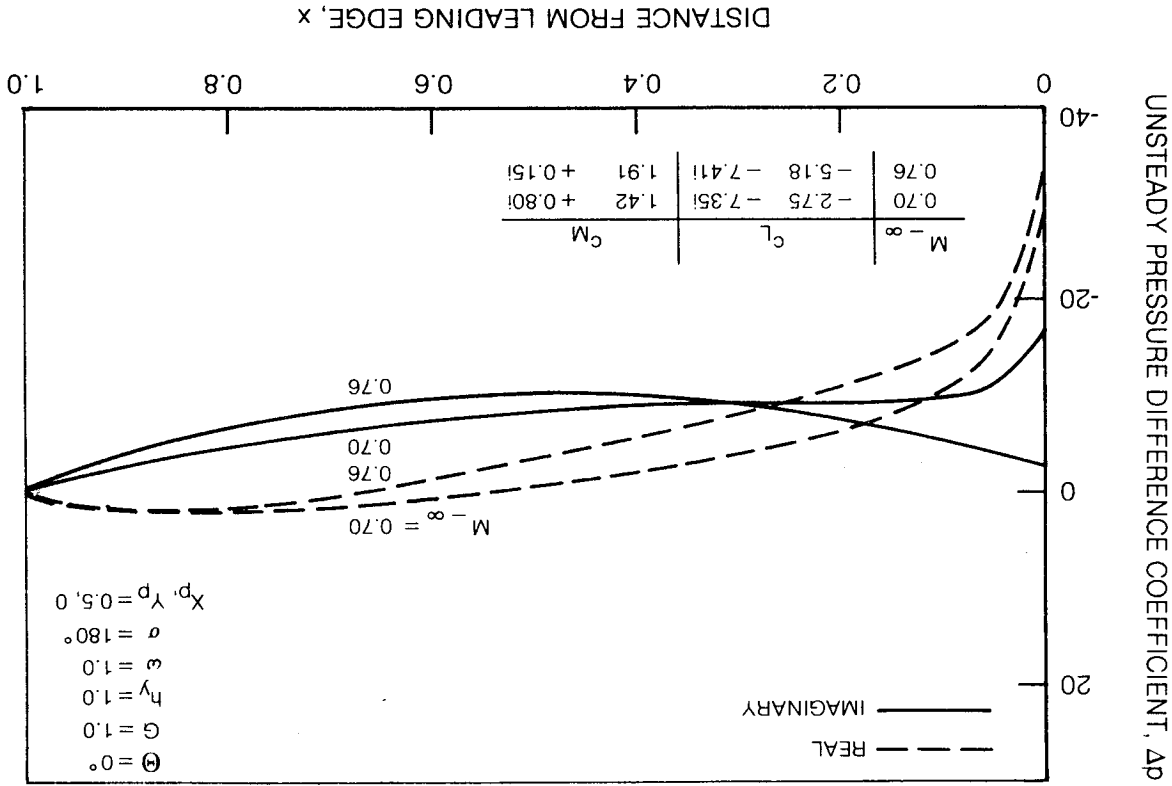| $M_{-\infty}$	c_L		c_M	
0.70	-9.00	$+1.65i$	1.09	$-1.93i$
0.76	-9.63	$+4.81i$	0.31	$-2.74i$

DISTANCE FROM LEADING EDGE, x

Fig. 15 Effect of Inlet Mach Number on Unsteady Response due to High-Frequency Torsional Vibrations of an Unstaggered Flat Plate Cascade
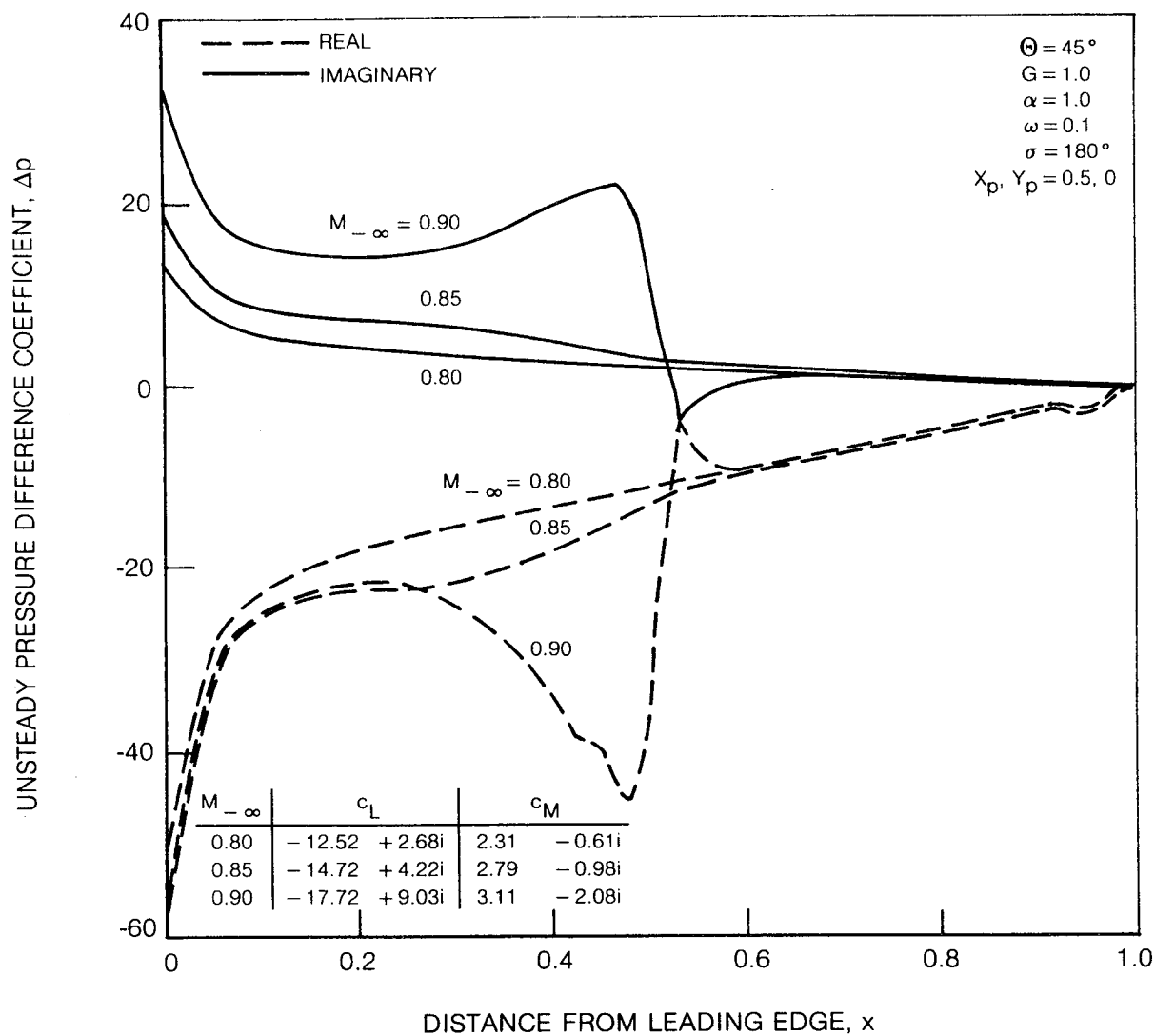
Fig. 16 Effect of Inlet Mach Number on Unsteady Response due to High-Frequency
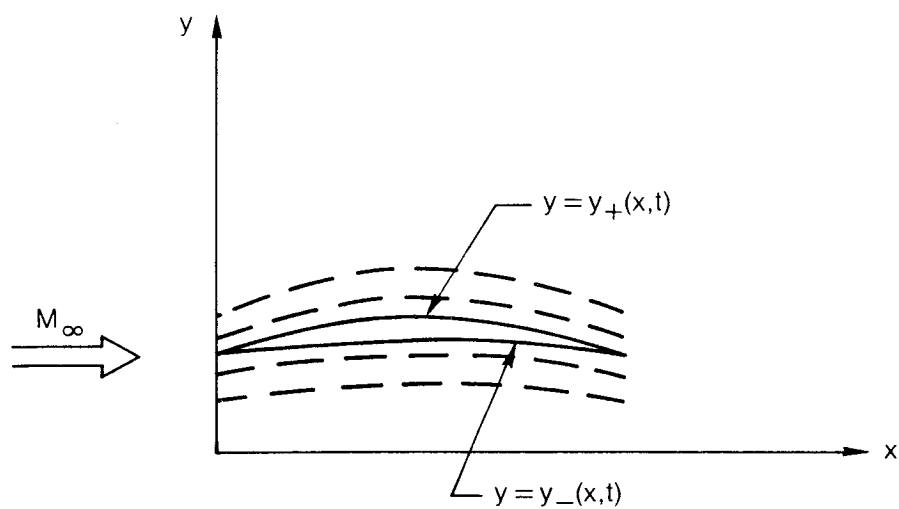Bending Vibrations of an Unstaggered DCA Cascade

Fig. 17 Effect of Inlet Mach Number on Unsteady Response due to High-Frequency Bending Vibrations of a Flat Plate Cascade

DISTANCE FROM LEADING EDGE, x

UNSTEADY PRESSURE DIFFERENCE COEFFICIENT, Δp

M_∞	c_L	c_M
0.70	−2.75 −7.35i	1.42 +0.80i
0.76	−5.18 −7.41i	1.91 +0.15i

0.76
0.70
0.76
$M_\infty = 0.70$

$X_p, Y_p = 0.5, 0$
$\sigma = 180°$
$\omega = 1.0$
$\gamma_h = 1.0$
$G = 1.0$
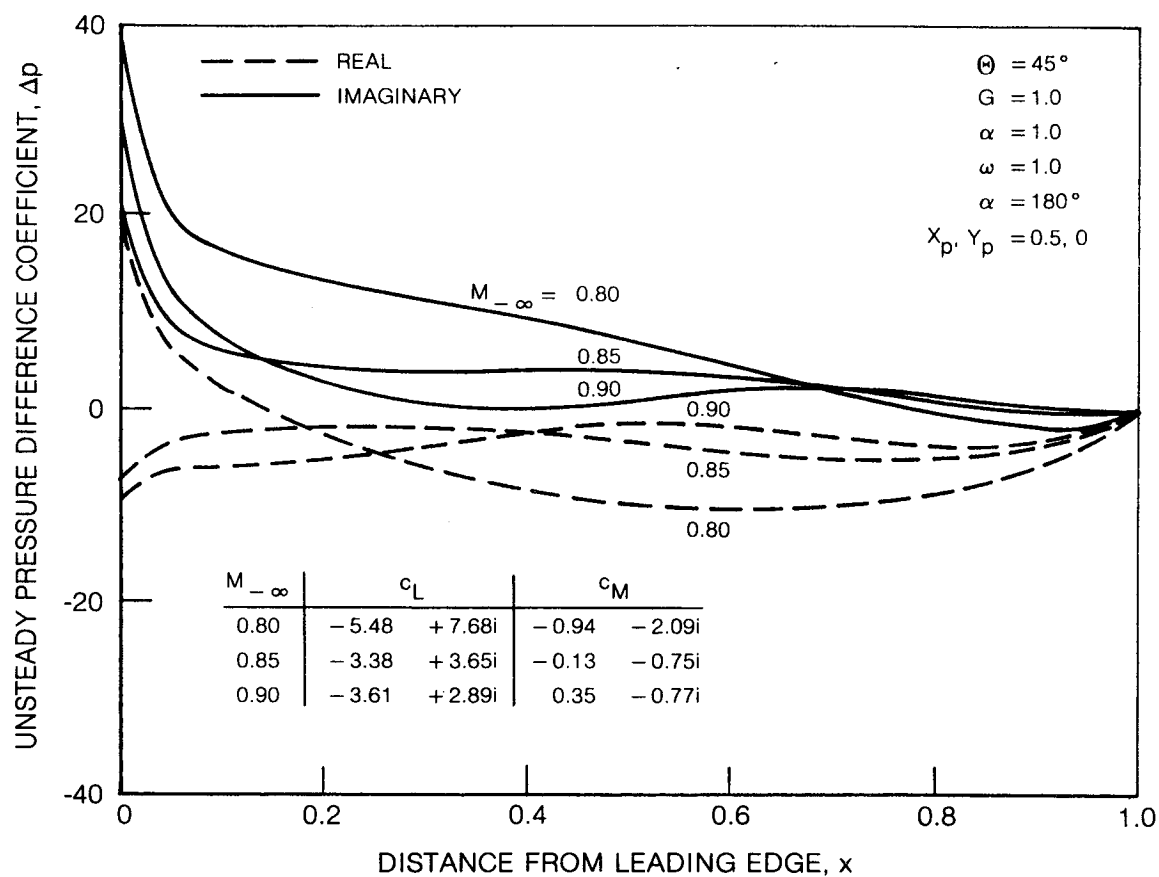$\Theta = 0°$

—— IMAGINARY
‑ ‑ ‑ REAL

Fig. 18 Effect of Inlet Mach Number on Unsteady Response due to Low-Frequency Torsional Vibrations of a Staggered DCA Cascade

Fig. 22 Thin Airfoil undergoing Small-Amplitude Motions Normal to the x-Axis

Fig. 21 Effect of Inlet Mach Number on Unsteady Response due to High-Frequency Torsional Vibrations of a Staggered Flat Plate Cascade

Fig. 20 Effect of Inlet Mach Number on Unsteady Response due to High-Frequency Torsional Vibrations of a Staggered DCA Cascade
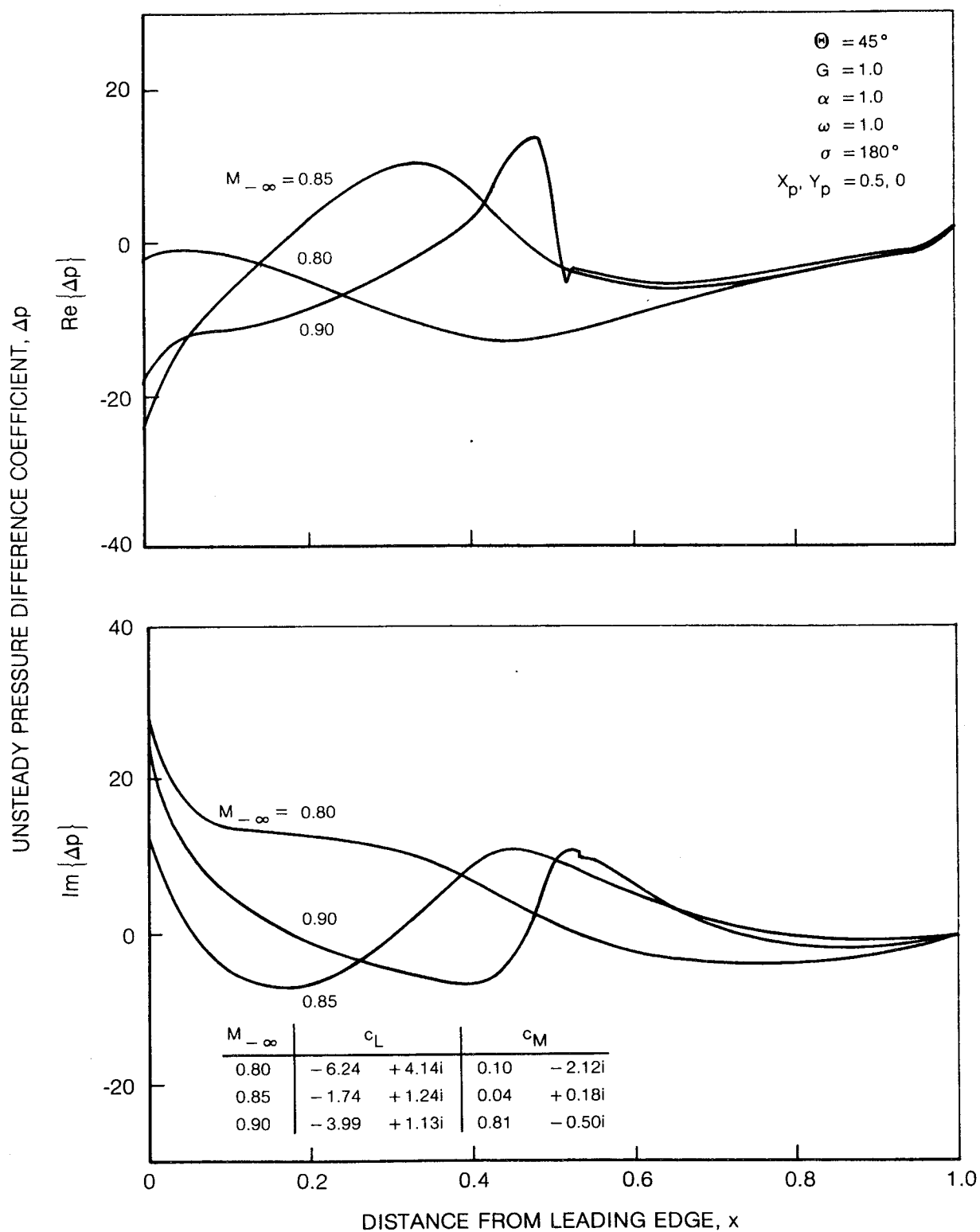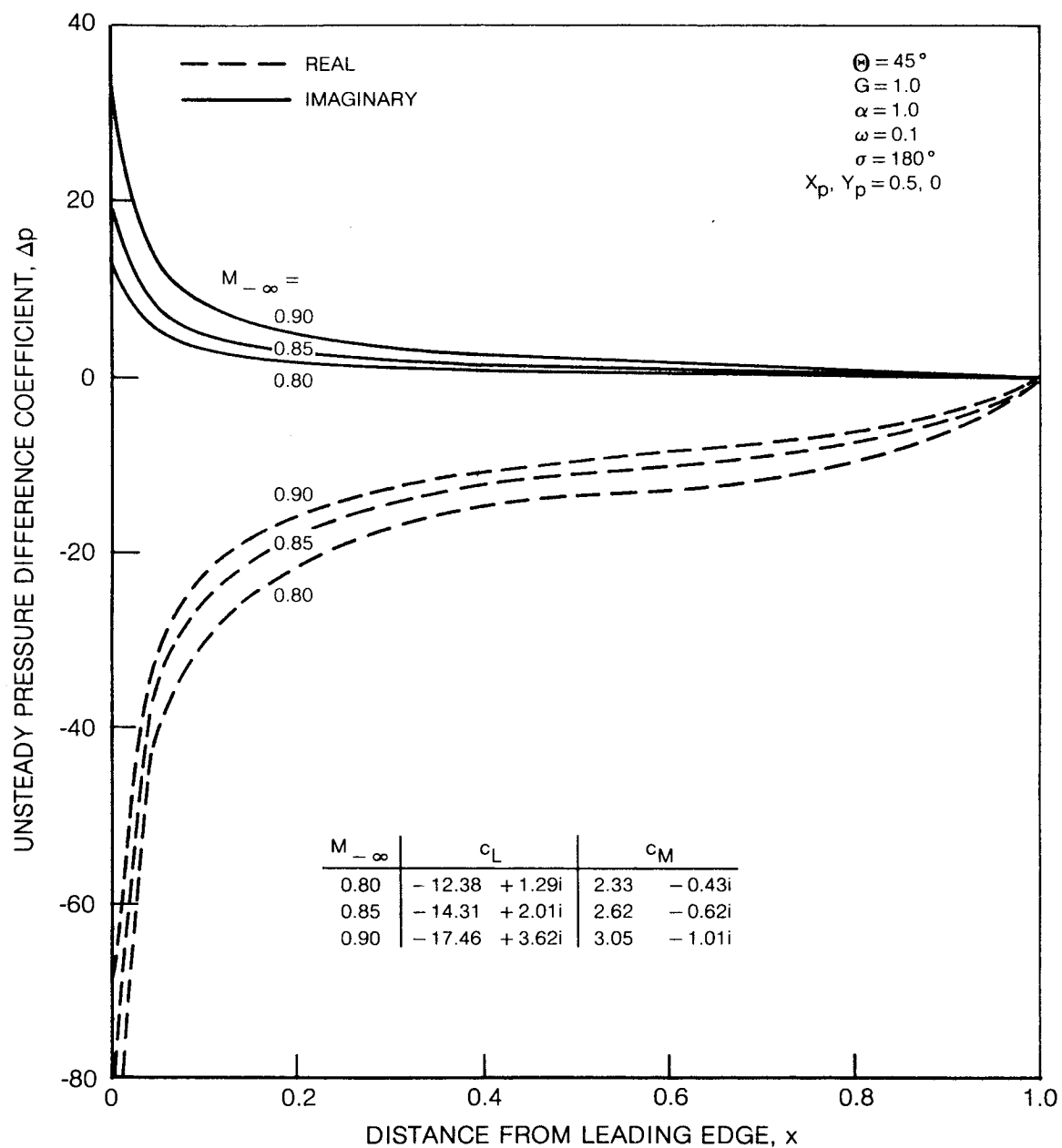
The figure shows two plots of unsteady pressure difference coefficient Δp versus distance from leading edge, x.

Parameters:
$\Theta = 45°$
$G = 1.0$
$\alpha = 1.0$
$\omega = 1.0$
$\sigma = 180°$
$X_p, Y_p = 0.5, 0$

Top plot: Re$\{\Delta p\}$ with curves for $M_{-\infty} = 0.85$, 0.80, 0.90

Bottom plot: Im$\{\Delta p\}$ with curves for $M_{-\infty} = 0.80$, 0.90, 0.85

Y-axis: UNSTEADY PRESSURE DIFFERENCE COEFFICIENT, Δp

X-axis: DISTANCE FROM LEADING EDGE, x

$M_{-\infty}$	c_L		c_M	
0.80	-6.24	$+4.14i$	0.10	$-2.12i$
0.85	-1.74	$+1.24i$	0.04	$+0.18i$
0.90	-3.99	$+1.13i$	0.81	$-0.50i$

82—9—10—1?

Fig. 19 Effect of Inlet Mach Number on Unsteady Response due to Low-Frequency Torsional Vibrations of a Staggered Flat Plate Cascade